Personalized stimulation therapies for disorders of consciousness: a computational approach to inducing healthy-like brain activity based on neural field theory

Journal of Neural Engineering

PAPER

Personalized stimulation therapies for disorders of consciousness: a computational approach to inducing healthy-like brain activity based on neural field theory

Daniel Polyakov[1], **P A Robinson**[2], **Eli J Müller**[3], **Glenn van der Lande**[4,5], **Pablo Núñez**[4,5,7], **Jitka Annen**[4,5,6], **Olivia Gosseries**[4,5,8] and **Oren Shriki**[1,8,*]

[1] Department of Cognitive and Brain Sciences, Ben-Gurion University of the Negev, Be'er-Sheva, Israel
[2] School of Physics, The University of Sydney, Sydney, NSW, Australia
[3] Brain and Mind Centre, The University of Sydney, Sydney, NSW, Australia
[4] Coma Science Group, GIGA Consciousness, University of Liège, Liège, Belgium
[5] NeuroRehab & Consciousness Clinic, Neurology Department, University Hospital of Liège, Liège, Belgium
[6] Department of Data Analysis, University of Ghent, Ghent, Belgium
[7] Biomedical Engineering Group, University of Valladolid, Valladolid, Spain
[8] These authors contributed equally to this work.
[*] Author to whom any correspondence should be addressed.

E-mail: shrikio@bgu.ac.il

Keywords: disorders of consciousness, brain stimulation, EEG, neural field theory

OPEN ACCESS

RECEIVED
14 November 2024

REVISED
15 April 2025

ACCEPTED FOR PUBLICATION
26 May 2025

PUBLISHED
10 June 2025

Abstract

Objective. Disorders of consciousness (DoC) remain a significant challenge in neurology, with traditional brain stimulation therapies showing limited and inconsistent efficacy across patients. This study presents a novel computational approach grounded in neural field theory for constructing personalized stimulus signals designed to induce healthy-like neural activity patterns in individuals with DoC. *Approach.* We employ a simplified brain model fitted to the electroencephalogram (EEG) power spectrum of a DoC patient, simulating the individual's neural dynamics. Using model equations and fitted parameters, we mathematically derive stimuli time series that cause the model to generate power spectra typical of healthy individuals. These stimuli are tailored for brain regions typically targeted by neuromodulation therapies, such as deep brain stimulation and repetitive transcranial magnetic stimulation. *Main results.* In silico simulations demonstrate that our method successfully induces healthy-like EEG power spectra in models fitted to DoC patients. Furthermore, when the model parameters were near a stability boundary, stimulation led to a bifurcation and lasting changes in the model's activity beyond the stimulation period. *Significance.* By inducing healthy-like neural activity, this approach may effectively activate plasticity mechanisms during long-term treatment, potentially leading to sustained improvements in a patient's condition. While further clinical adjustments and validation are needed, this method holds promise for improving therapeutic outcomes in DoC. Moreover, it offers potential extensions to other neurological conditions that could benefit from personalized brain stimulation therapies.

1. Introduction

1.1. Disorders of consciousness

Disorders of consciousness (DoC) encompass a range of conditions characterized by impaired awareness and wakefulness resulting from severe brain damage. These conditions include coma, unresponsive wakefulness syndrome (UWS), and minimally conscious state (MCS). Collectively, these conditions disrupt the intricate neural processes that underlie human consciousness irrespective of arousal, challenging our fundamental understanding of how the brain forms awareness, and cognition, thereby prompting profound scientific, clinical, and ethical inquiries [1, 2].

DoC can originate from a variety of causes, such as traumatic brain injuries, anoxia, strokes, and intoxication. These conditions lead to impairments in a persons' awareness and in their ability to respond

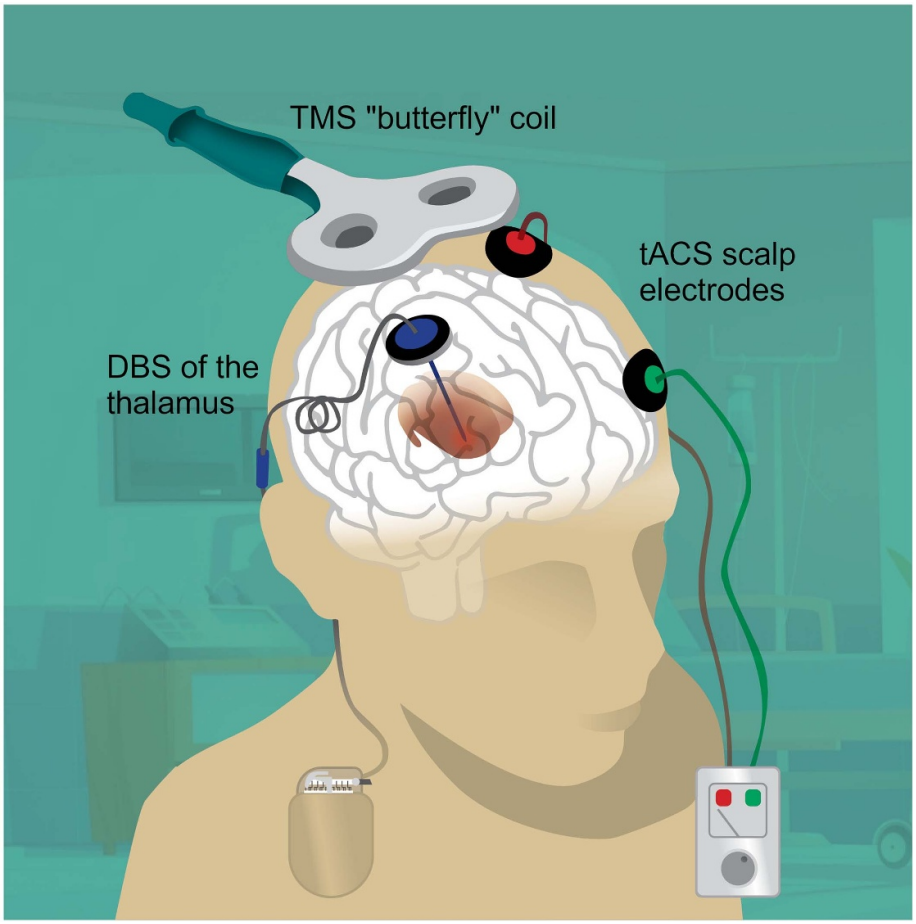

Figure 1. Example of various brain stimulation methods applied to a patient. Deep brain stimulation (DBS) involves the implantation of electrodes into specific brain areas that deliver controlled electrical impulses. Transcranial magnetic stimulation (TMS) utilizes magnetic pulses that are directed through the patient's skull. Transcranial alternating current stimulation (tACS) transmits alternating electrical current between two electrodes (or more) positioned on the patient's scalp. (This figure includes a hospital background image by Upklyak from Freepik.).

to the external environment [1]. However, in clinical practice, the assessment of a patient's state of consciousness is primarily based on their responsiveness. For DoC assessment of the level of consciousness, the Coma Recovery Scale-Revised (CRS-R) is typically used. It assesses auditory, visual, motor, oromotor, communication, and arousal functions. Each function contributes points to a total score ranging from 0 (coma) to 23 (emergence from MCS), reflecting overall severity. Diagnosis of specific DoC states relies on achieving specific response levels within each item category, such as visual pursuit or command response, or by using a CRS-R index based on the highest item in every category [3, 4].

The consciousness state of DoC patients can be enhanced through various therapeutic approaches. These approaches include neurorehabilitation strategies, surgical procedures, pharmacological interventions, brain stimulation, and emerging experimental treatments such as stem-cell therapy [5–7]. In this context, our focus is on brain stimulation, specifically the use of electrical or magnetic stimulation to modify brain activity, in order to promote neural plasticity and to re-activate damaged brain circuits [8–10].

1.2. Brain stimulation therapies

Various stimulation therapies have been explored as potential interventions to improve outcomes in individuals with DoC, focusing particularly on those with UWS or MCS. Techniques such as deep brain stimulation (DBS), transcranial magnetic stimulation (TMS), transcranial direct current stimulation (tDCS), transcranial alternating current stimulation (tACS), and vagus nerve stimulation (VNS) have been applied to DoC patients to increase cortical excitability and, consequently, to enhance consciousness (see figure 1) [6, 9, 11].

Among invasive therapies, DBS requires surgically implanting electrodes into specific brain regions to deliver controlled electrical impulses, showing promise in improving consciousness among individuals with DoC. Stimulation of various thalamic nuclei has demonstrated significant success rates, with sustained improvements observed in numerous patients [12–16]. VNS therapy, involving stimulation of the

vagus nerve, offers a less invasive alternative, potentially modulating consciousness by influencing corticothalamic networks and the reticular activation system via connections with the brainstem [17]. Despite limited spatial precision, VNS has shown a sustained improvement in the level of consciousness in MCS patients [9, 18].

TMS is a non-invasive technique that involves delivering magnetic fields through the skull to induce electrical currents in specific brain regions. Repetitive TMS (rTMS) [19] has demonstrated efficacy in enhancing behavioral scores among DoC patients. However, its efficacy varies among individuals, and long-term benefits remain uncertain [9, 11, 20]. In both tDCS and tACS, mild electrical current is transmitted through the scalp, with the former aiming to modify cortical excitability and the latter seeking to synchronize with brain oscillations. Evidence indicates that tDCS can lead to significant improvements in CRS-R scores, but like rTMS, the long-term efficacy and effects of tDCS are subjects of ongoing research [6, 9, 11]. As for tACS, there is not enough research to draw conclusions about its effectiveness for the treatment of DoC [21]. Notably, all of these non-invasive techniques typically target the dorsal prefrontal cortex, which is part of a network associated with consciousness in the brain [9, 20–22].

Despite the potential of these brain stimulation methods, their adoption as reliable therapies for DoC faces challenges due to the considerable variability in treatment outcomes, attributed to factors like the patient's condition, the extent of brain damage, and individual biological characteristics [9, 16]. In turn, this leads to a large variability in the patients' need in stimulation, from the most appropriate technique (e.g. transcranial, or more invasive DBS), to stimulation parameters in terms of e.g. location, frequency, and duration. With the large heterogeneity and low sample sizes, finding a common, effective stimulation paradigm has major feasibility challenges. Computational modeling is an outstanding tool in overcoming these shortcomings, because without increased burden for the patient, a search for optimal stimulation could be conducted. To address this issue, we aim to provide a road to improvement in these issues by modeling an abstract representation of the discussed stimulation techniques and focusing on tailoring the electromagnetic signal for specific patients. This stimulation approach is coupled to a physiologically-inspired brain model capable of representing the patient's own brain activity. By tailoring the stimulation to each patient's unique profile, we hope to demonstrate how modeling could be utilized in the future to deal with the DoC population's heterogeneity that could affect treatment effectiveness.

1.3. Multiscale brain modeling

Over the past half-century, significant progress has been made in the development of brain activity models that address various phenomena across different brain regions and spatial scales. In particular, efforts have been directed toward creating comprehensive multiscale models of whole-brain activity that are capable of simulating various phenomena and generating realistic signals. One noteworthy modeling framework, 'The Virtual Brain', employs neural mass models to represent brain regions interconnected based on connectome data. This model demonstrates the capacity to simulate diverse phenomena, including epilepsy and sleep stages. Nevertheless, fitting it to experimental data remains challenging because the use of non-linear differential equations is required to generate the activity of each region [23, 24]. Another approach, the 'Multiscale Neural Model Inversion' framework, focuses on effective connectivity. It constructs interregional networks based on structural connectivity and fits their activity to functional magnetic resonance imaging data through functional connectivity correlation, ultimately generating blood-oxygen-level-dependent signals similar to those that are observed in pathologies like major depression and Alzheimer's disease. However, the output aligns only with the first and second moments of the experimental data, thereby capturing only the fundamental properties of the simulated phenomena [25]. In contrast, neural field theory (NFT) modeling offers an efficient approach to building networks of interconnected brain regions that interact through physiologically-based wave equations, thereby capturing both stationary and transient neural activity. NFT has demonstrated success in representing consciousness-related phenomena like sleep stages and epilepsy and has presented substantial capabilities of classifying states of consciousness [26–30]. Furthermore, the NFT framework provides convenient tools for fitting and simulating neural activity using standard computing equipment [28, 31].

Moreover, it is important to note that NFT has previously been employed to model various stimulation techniques and their impacts on both healthy and pathological brains. For instance, Wilson *et al* used NFT to model the effects of TMS on calcium-dependent synaptic plasticity in long-term potentiation and depression processes [32, 33]. Müller and Robinson applied NFT to model the effects of DBS on Parkinson's disease, including a detailed model of the corticothalamic-basal ganglia system that replicated key clinical features of the disease, such as high beta-activity. They explored different DBS protocols and successfully demonstrated their ability to reduce beta-activity in the model [34, 35]. Müller *et al* also investigated consciousness modulation through DBS by simulating the expression of propofol anesthesia in a corticothalamic system and introducing a stimulus to the matrix thalamus. Their model demonstrated arousal from anesthesia, characterized by wake-like dynamics that facilitated high information transfer

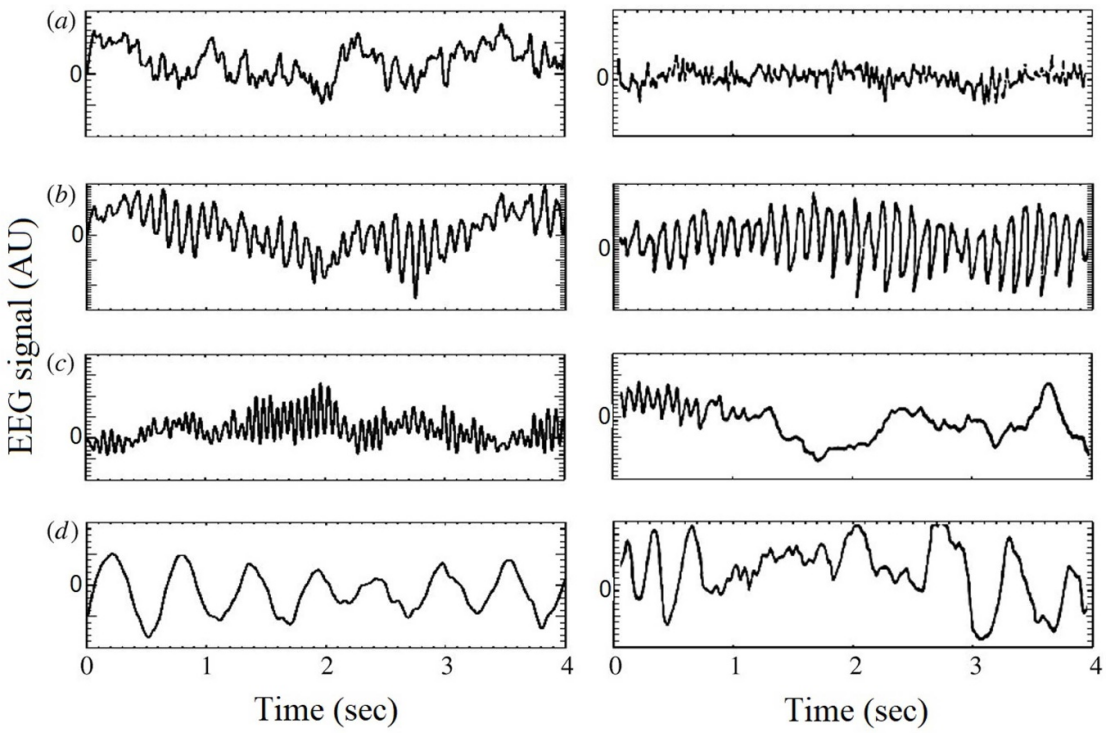

Figure 2. Simulated vs. experimental EEG time series of waking and sleeping states. In the left panels: NFT-generated time series of (a) resting state—open eyes, (b) resting state—closed eyes, (c) quiescent sleep (non-REM) stage 2, and (d) quiescent sleep stage 3. In the right panels: corresponding time series from human subjects. The time series were scaled and displayed in arbitrary units (AU) for visualization purposes [48, 49]. Reproduced with permission from [26]. © 2005 The Royal Society.

[36]. Thus, NFT appears to be a suitable framework for developing personalized stimulation signals for DoC patients. Furthermore, it offers the capability to incorporate these signals into the modeled stimulation techniques mentioned here or those that may be modeled in the future.

1.4. Proposed approach

As previously mentioned, our approach aims to establish a systematic method for constructing patient-specific and region-specific stimulation signals. The core idea involves utilizing a corticothalamic NFT model (CTM) capable of simulating both healthy-like and DoC-like neural activity, while allowing for targeted stimulation of the modeled regions. We fit this model to a specific DoC patient, and then we mathematically derive the stimulus signal required to induce typical healthy-like neural activity within the model. The fitting of the model and the construction of the stimulus signal rely on the corresponding electroencephalogram (EEG) power spectra, aiming to generate a healthy-like power spectrum. We apply the constructed signal to brain regions typically targeted by DBS, rTMS, and tACS, and successfully demonstrate the effectiveness of our method *in silico*.

Our approach holds promise for application in DBS, rTMS, and tACS, as they demonstrated the ability to influence various bands of DoC patients' power spectrum [13, 21, 37]. Conversely, tDCS is not well-suited for our approach because it only allows for amplitude adjustment, which is insufficient for independently controlling the power of different frequencies. Moreover, since the brainstem and vagus nerve are not included in the CTM, we did not construct a signal for application in VNS in this study. Generally, with appropriate adaptations and clinical verifications, this method has the potential to significantly advance a wide range of brain stimulation therapies, offering a personalized approach that could lead to more effective and longer-lasting treatments for DoC.

2. Materials and methods

2.1. Neural field theory

Neural-field theory [26, 38, 39] is a family of large-scale brain models rooted in physiological principles, that can replicate a wide range of brain activities across multiple scales. This methodology models a continuum of corticothalamic activity by incorporating population-specific local dynamics and employing wave equations to characterize interactions between these populations [40]. Consequently, it effectively replicates and integrates numerous phenomena observed in EEG data, including spectral peaks observed during waking and sleeping states, event-related potentials, measures of connectivity,

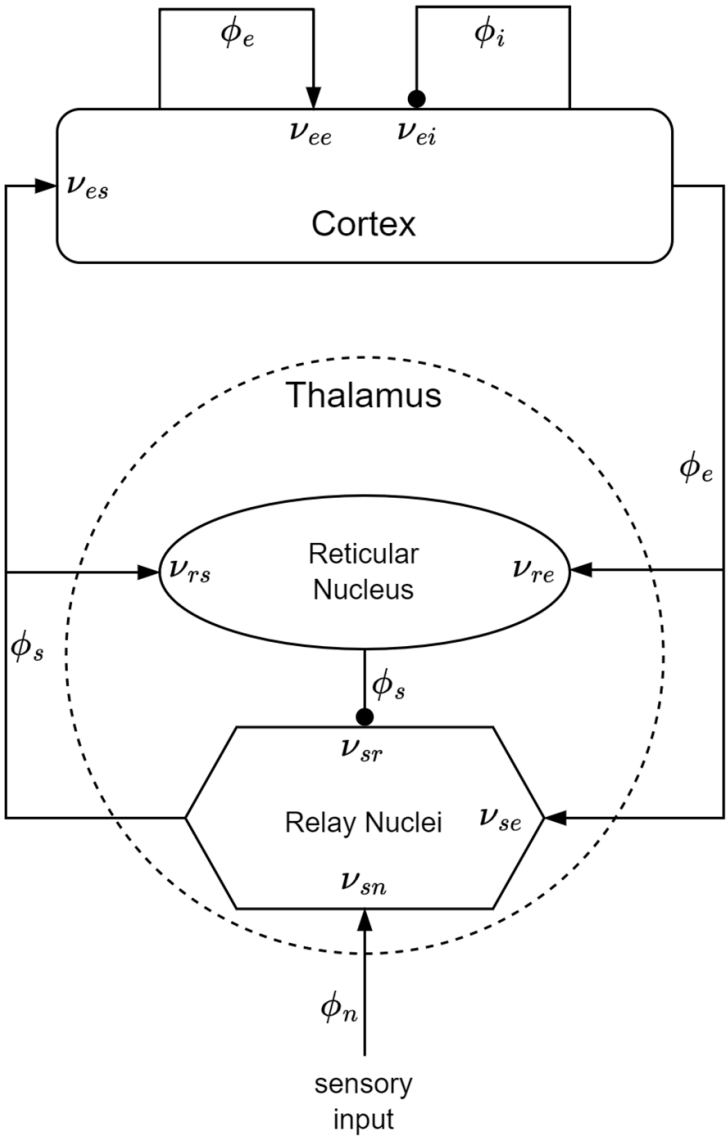

Figure 3. Schematic representation of the corticothalamic NFT model (CTM). Shown are the four neural populations: cortical excitatory *e*, and inhibitory *i*, thalamic relay nuclei *s*, and thalamic reticular nucleus *r*. The connection strength from population *b* to population *a* is represented by the parameter ν_{ab}. Excitatory connections are represented by pointed arrowheads, and inhibitory connections by round arrowheads.

and spatiotemporal structure, and even the dynamics of epileptic seizures (see figure 2) [27, 41–47]. Model parameters have biophysical meaning and include synaptic strengths, excitatory and inhibitory gains, synaptic and dendritic time constants, propagation delays, and axonal ranges. NFT's whole-brain modeling is a bottom-up method, effectively complementing cellular and local network analyses by averaging microstructure into mean-field equations. Additionally, NFT's strength lies in its dynamic analysis, which explores the model's states and their stability in relation to changes in model parameters [28, 45, 46].

The neural field, denoted as $\phi(\mathbf{r}, t)$ $[\mathrm{s}^{-1}]$ represents a spatiotemporal neural activity that propagates among neural populations when averaged over scales of approximately 0.1 millimeters. The CTM comprises four neural populations, interconnected as illustrated in figure 3. These populations include excitatory (e) and inhibitory (i) cortical neurons, thalamic relay nuclei neurons (s), thalamic reticular nucleus neurons (r), and sensory inputs (n). The soma potential of each population, $V_a(\mathbf{r}, t)$ [V], is influenced by contributions ϕ_b from presynaptic populations and ultimately generates outgoing neural activity $\phi_a(\mathbf{r}, t)$.

The dendritic spatiotemporal potential V_{ab} [V] relates to the input ϕ_b via equation (1). Connection strength from population b to a is defined by $\nu_{ab} = s_{ab}N_{ab}; [\mathrm{V} \cdot \mathrm{s}]$, where N_{ab} represents the mean number of synapses per neuron a originating from neurons of type b, and s_{ab} $[\mathrm{V} \cdot \mathrm{s}]$ is the mean time-integrated strength of the soma response for each incoming spike. The parameter τ_{ab} [s] specifies the one-way

corticothalamic time delay, while $D_a(t)$ is a differential operator, as defined in equation (2). The quantities $1/\alpha$ and $1/\beta$ indicate the decay time and rise times of the soma response in the corticothalamic system, respectively.

Dendritic component:

$$D_a(t)\,V_{ab}(\mathbf{r},t) = \nu_{ab}\phi_b(\mathbf{r},t-\tau_{ab}) \tag{1}$$

$$D_a(t) = \frac{1}{\alpha\beta}\frac{\mathrm{d}^2}{\mathrm{d}t^2} + \left(\frac{1}{\alpha}+\frac{1}{\beta}\right)\frac{\mathrm{d}}{\mathrm{d}t} + 1 \tag{2}$$

The soma potential, V_a, emerges as the aggregate of its dendritic potentials, as detailed in equation (3). This potential undergoes some smoothing due to synaptodendritic dynamics and soma capacitance. Additionally, the population generates spikes at an average firing rate $Q_a\,[\mathrm{s}^{-1}]$, which is linked to the soma potential via a sigmoid function $S(V_a)$ (relative to the resting state), as specified in equation (4). Within this equation, $Q_{\max}$ represents the maximum firing rate. The quantities θ and $\sigma' \cdot \pi/\sqrt{3}$ correspond to the mean and the standard deviation (SD), of the firing threshold voltage, respectively.

Soma component:

$$V_a(\mathbf{r},t) = \sum_b V_{ab}(\mathbf{r},t) \tag{3}$$

$$Q_a = S(V_a) = \frac{Q_{\max}}{1+e^{-(V_a-\theta)/\sigma'}} \tag{4}$$

The field ϕ_a approximately adheres to a wave equation with dampening, incorporating a source term Q_a, as specified in equation (5). The differential operator $D_a(\mathbf{r},t)$ defined in equation (6), incorporates parameters: $\nu_a\,[\mathrm{m}\cdot\mathrm{s}^{-1}]$ capturing the wave's propagation velocity, $r_a\,[\mathrm{m}]$ indicating the mean propagation range, and $\gamma_a = \nu_a/r_a\,[\mathrm{s}^{-1}]$ representing the damping rate.

Axonal component:

$$D_a(\mathbf{r},t)\,\phi_a(\mathbf{r},t) = Q_a(\mathbf{r},t) \tag{5}$$

$$D_a(\mathbf{r},t) = \frac{1}{\gamma_a^2}\frac{\partial^2}{\partial t^2} + \frac{2}{\gamma_a}\frac{\partial}{\partial t} + 1 - r_a^2\nabla^2 \tag{6}$$

In the CTM, only r_e exhibits sufficient magnitude to generate significant propagation dynamics. As a result, the fields of other populations can be approximated as $\phi_a(\mathbf{r},t) = S[V_a(\mathbf{r},t)]$. Additionally, it is assumed that the only nonzero time delays between populations are τ_{es}, τ_{is}, τ_{se}, and $\tau_{re} = t_0/2$, with t_0 representing the total traversal time through the corticothalamic loop. Notably, equation (5) inherently captures corticocortical time delays through its wave equation formulation. To streamline the model, we adopt an assumption of random intracortical connectivity, which establishes $N_{ib} = N_{eb}$ across all b [50]. This premise implies that the connection strengths are symmetric, resulting in $\nu_{ee} = \nu_{ie}$, $\nu_{ei} = \nu_{ii}$, and $\nu_{es} = \nu_{is}$ [26, 28]. Utilizing numerical integration [31] or analytical integration when possible [51], the NFT equations generate a spatiotemporal activity signal that propagates across the cortical surface.

2.2. EEG power spectrum generated from the CTM

In instances of spatially uniform steady-state activity, an analytical computation of the model's power spectrum becomes feasible, circumventing the need for numerical integration. Achieving the steady state involves setting all temporal and spatial derivatives to zero. By utilizing the first term of the Taylor expansion, a linear approximation of all potential steady-state perturbations can be derived. Under these conditions, a Fourier transform of the model equations yields equation (7) for the dendritic component and equation (8) for the axonal component. Within these equations, $\omega = 2\pi f$ represents the angular frequency, $k = 2\pi/\lambda$ indicates the wave vector (λ is the wavelength), and $V_a^{(0)}$ denotes the steady-state potential [28].

The dendritic component in the frequency domain:

$$V_{ab}(\mathbf{k},\omega) = \nu_{ab}\phi_b(\mathbf{k},\omega)\,L(\omega)\,e^{i\omega\tau_{ab}}$$
$$L(\omega) = \left(1-\frac{i\omega}{\alpha}\right)^{-1}\left(1-\frac{i\omega}{\beta}\right)^{-1} \tag{7}$$

The axonal component in the frequency domain:

$$D_a(\mathbf{k},\omega)\cdot\phi_a(\mathbf{k},\omega) = \rho_a V_a(\mathbf{k},\omega)$$
$$D_a(\mathbf{k},\omega) = k^2 r_a^2 + \left(1-\frac{i\omega}{\gamma_a}\right)^2$$
$$\rho_a = \frac{\mathrm{d}S\left(V_a^{(0)}\right)}{\mathrm{d}V_a} \tag{8}$$

Utilizing equation (3), we can present equation (8) as:

$$D_a(\mathbf{k},\omega)\cdot\phi_a(\mathbf{k},\omega) = \rho_a\sum_b V_{ab}(\mathbf{k},\omega) = \sum_b J_{ab}\phi_b(\mathbf{k},\omega)$$
$$J_{ab} = \rho_a\nu_{ab}L(\omega)\,e^{i\omega\tau_{ab}} = G_{ab}L(\omega)\,e^{i\omega\tau_{ab}} \tag{9}$$

Then we can represent the interactions between the different CTM populations in matrix notation:

$$\begin{bmatrix} D_e & 0 & 0 & 0 \\ 0 & D_i & 0 & 0 \\ 0 & 0 & D_r & 0 \\ 0 & 0 & 0 & D_s \end{bmatrix}\cdot\begin{bmatrix}\phi_e\\ \phi_i\\ \phi_r\\ \phi_s\end{bmatrix} = \begin{bmatrix} J_{ee} & J_{ei} & 0 & J_{es} \\ J_{ie} & J_{ii} & 0 & J_{is} \\ J_{re} & 0 & 0 & J_{rs} \\ J_{se} & 0 & J_{sr} & 0 \end{bmatrix}\cdot\begin{bmatrix}\phi_e\\ \phi_i\\ \phi_r\\ \phi_s\end{bmatrix} + \begin{bmatrix}0\\0\\0\\ J_{sn}\phi_n\end{bmatrix} \tag{10}$$

Equation (10) admits an alternative, more concise representation, where $\mathbf{J}^\star\boldsymbol{\phi}^\star$ denotes the external input to the CTM:

$$\mathbf{D}\boldsymbol{\phi} = \mathbf{J}\boldsymbol{\phi} + \mathbf{J}^\star\boldsymbol{\phi}^\star \tag{11}$$

$$\phi_e(\mathbf{k},\omega) = \frac{G_{es}G_{sn}L^2 e^{\frac{i\omega t_0}{2}}}{(1-G_{srs}L^2)(1-G_{ei}L)(k^2r_e^2+q^2r_e^2)}\phi_n(\mathbf{k},\omega) \equiv \Psi(\mathbf{k},\omega)\phi_n(\mathbf{k},\omega)$$
$$q^2r_e^2 = \left(1-\frac{i\omega}{\gamma_e}\right)^2 - \frac{1}{1-G_{ei}L}\left\{LG_{ee} + \frac{\left[L^2G_{ese}+L^3G_{esre}\right]e^{i\omega t_0}}{1-L^2G_{srs}}\right\} \quad (12)$$

By solving equation (10), taking into account all the previously established assumptions regarding D_a, ν_{ab}, and τ_{ab}, we can derive equation (12). In this framework, the quantities $G_{ese} = G_{es}G_{se}$, $G_{esre} = G_{es}G_{sr}G_{re}$, and $G_{srs} = G_{sr}G_{rs}$ represent the overall gains for the excitatory corticothalamic, inhibitory corticothalamic, and intrathalamic loops, respectively. The firing rate of sensory inputs to the thalamus, ϕ_n, is modeled as white noise. For computational convenience, $\phi_n(\omega)$ can be set to 1, while only G_{sn} is subject to variation The excitatory field ϕ_e is considered a good approximation of scalp EEG signals [28]. The EEG power spectrum $P(\omega)$ (equation (13)) is derived by integrating $|\phi_e(\mathbf{k},\omega)|^2$ across $\mathbf{k}$ with the cortex modeled as a rectangular sheet of dimensions $L_x \times L_y$. Under periodic boundary conditions, this integration transitions into a summation across spatial modes with discretized k. The filter function $F(k)$ provides a computational approximation of the low-pass spatial filtering resulting from volume conduction through cerebrospinal fluid, skull, and scalp layers

$$P(\omega) = \sum_{m=-\infty}^{\infty}\sum_{n=-\infty}^{\infty} |\phi_e(k_x,k_y,\omega)|^2 F(k)\Delta k_x \Delta k_y$$
$$k_x = \frac{2\pi m}{L_x}, k_y = \frac{2\pi n}{L_y}, k = \sqrt{k_x^2+k_y^2}$$
$$F(k) = e^{-k^2/k_0^2} \quad (13)$$

By merging equation (13) with equation (12), we can formulate the expression for the power spectrum of the CTM. Given that ϕ_n is equal for every k, we can write it as $\phi_n(\omega)$ outside the summation

$$P(\omega) = \sum_{m=-\infty}^{\infty}\sum_{n=-\infty}^{\infty} |\Psi(\mathbf{k},\omega)\phi_n(\mathbf{k},\omega)|^2 F(k)\Delta k_x \Delta k_y \equiv |\phi_n(\omega)|^2 \cdot U(\omega) \quad (14)$$

2.2.1. Model fitting and signal generation

The analytical form of the CTM power spectrum, as expressed in equation (14), can be fitted to the experimental EEG power spectrum. This fitting process is carried out through a Monte-Carlo Markov-Chain optimization procedure applied to model parameters, a method implemented in the *braintrak* toolbox [28]. Here, we optimize the following model parameters: G_{ee}, G_{ei}, G_{es}, G_{se}, G_{sr}, G_{sn}, G_{re}, G_{rs}, α, β, t_0, and EMG_a. To support multi-electrode fitting, we assumed that G_{ee}, G_{ei}, G_{sn}, α,β, and t_0 exhibit a cosine-like variation over the scalp [40]. Subsequently, time series were generated from the fitted model by numerically integrating its partial differential equations over time, incorporating the *NFTsim* toolbox [31]. An illustrative example showing an experimental EEG Cz electrode power spectrum, a power spectrum derived from the fitted model, and a simulated EEG Cz electrode power spectrum is depicted in figure 4. The Cz electrode was specifically chosen to illustrate spectra of simulated data throughout this work, as its activity effectively represents the overall EEG activity generated by the CTM.

2.3. Stimulus construction workflow

We recruited NFT equations and a framework to derive a stimulus signal that would cause a CTM fitted to a specific DoC patient to produce a power spectrum similar to that of a healthy individual. Here is an outline of the proposed workflow:

1. Compute the EEG power spectra of a typical healthy subject $P_{\mathrm{EXP}}^{\mathrm{hlt}}(\omega)$ and a specific DoC patient $P_{\mathrm{EXP}}^{\mathrm{doc}}(\omega)$.
2. Fit CTMs to both the healthy subject and DoC patient, determine models' parameters, and obtain the corresponding power spectra, $P^{\mathrm{hlt}}(\omega)$ and $P^{\mathrm{doc}}(\omega)$.
3. Compute the stimulus time series $\phi^{\mathrm{stim}}(t)$ by solving $P^{\mathrm{hlt}}(\omega) = P^{\mathrm{doc+stim}}(\omega)$. (The solutions for the

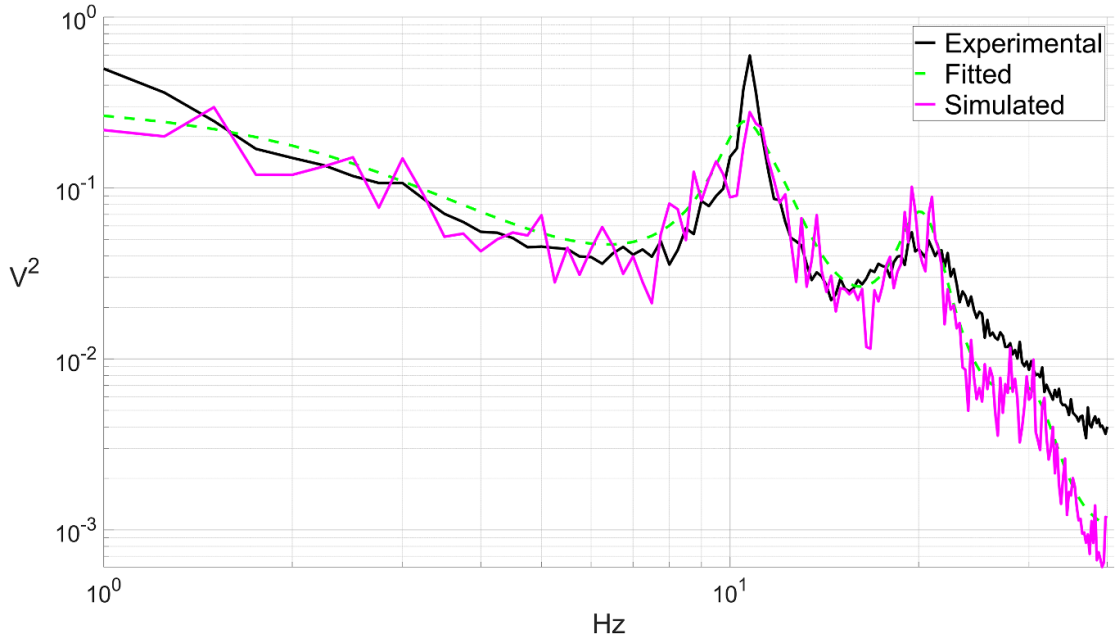

Figure 4. Experimental, fitted, and simulated power spectra. Example of a Cz electrode EEG power spectrum of a healthy subject (black curve), a fitted CTM power spectrum (green dashed curve), and a Cz electrode power spectrum of a simulated EEG (purple curve).

stimuli applied to the different populations of the CTM are provided further in table 2). Present the time series as a Fourier series to support continuous stimulation.

We evaluate the effectiveness of the calculated stimulation signal by generating EEG time series from models with 'Healthy-fitted' and 'DoC-fitted with stimulation' parameters. We then compare $P_{\mathrm{SIM}}^{\mathrm{hlt}}$ and $P_{\mathrm{SIM}}^{\mathrm{doc+stim}}$ both visually and by computing the Pearson correlation between their power spectra. It is worth noting that we can also choose to skip the fitting of the model to the healthy subject and use the experimental power spectrum $P_{\mathrm{EXP}}^{\mathrm{hlt}}(\omega)$ directly, as the stimulus-specific equations do not rely on the healthy-fitted CTM. We present both approaches in our results, providing flexibility in the experimental design.

2.3.1. Experimental data

In our research, we utilized a dataset consisting of open-eyes resting-state EEG recordings acquired from DoC patients, as well as from healthy controls. Each participant's EEG activity was recorded using a Hydro-Cel GSN high-density electrode net (Electric Geodesics, EGI) equipped with 256 electrodes, with a sampling rate of 250 Hz. Data collection took place in a controlled environment, characterized by darkness and minimal sensory stimuli, with EEG recording sessions lasting approximately 30 min. Behavioral assessments using the CRS-R were performed several times within a few days, including just before the EEG acquisition [52].

We chose an MCS patient (a 29-year-old male with a history of traumatic brain injury, CRS-R score of 9, and 181 months since the injury) and a UWS patient (a 31-year-old female with a history of brain hemorrhage, CRS-R score of 6, and 45 months since the injury) along with four healthy subjects (#1: a 62-year-old male; #2: a 19-year-old male; #3: a 40-year-old female; #4: a 53-year-old male) to present the application of our method. It is important to emphasize that these subjects were chosen for illustrative purposes only, and our approach is applicable to any pair of subjects, as shown further [53].

Each subject's EEG data went through several processing steps. First, we kept only 137 central electrodes and removed the rest in order to focus only on scalp-based electrodes. The signals from these electrodes were high-pass filtered above 0.2 Hz and notched at 50 Hz to eliminate line noise. Subsequently, to streamline computational processes, they were down-sampled to 125 Hz. The 30 min recording was then partitioned into nearly stationary sections (required for CTM fitting, which is performed through steady-state activity power spectrum), with durations varying from 2.5 to 10 min. Detecting potential onsets of stationary sections involved splitting the electrode signals into 10 s segments and identifying when the segment's SD deviated by two SDs compared to the preceding segment. Defining stationary section boundaries required simultaneous onsets in more than 5% of the electrodes, with at least 2.5 min between onsets. Sections lasting between 10 and 20 min were equally divided into two, while

those between 20 and 30 min were split into three sections.

The cleaning process for each stationary section of the data involved several sequential steps. Initially, noisy channels (electrode signals) were identified by segmenting the data into 5 s segments and calculating the SD of each channel within a segment. A channel within a segment was flagged as noisy if its SD exceeded seven times the SD of the entire non-segmented channel, or if it was three times higher than that of the other channels within the same segment. Segments with at least one noisy channel were deemed noisy, and entire channels were marked as noisy if more than 33% of their segments exhibited noise. These identified entire noisy channels were then removed and replaced with channels generated through a spherical spatial interpolation of the remaining channels. Subsequently, the data was re-referenced to the average of all channels and any remaining artifacts were eliminated. Artifacts were defined as 1 s segments where any sample's SD was five times greater than the channel's entire SD. To further refine the data, we conducted an independent component analysis to isolate and remove components associated with eye movements and non-EEG activity. After decomposition, we employed the *IClabel* toolbox [54] to retain only those components identified with at least 50% confidence as originating from genuine neural activity. The steps involving spatial interpolation, average referencing, and independent component analysis were all executed using the *EEGLAB* toolbox [55].

From the various stationary sections of each subject, we retained sections where fewer than 10% of the channels were flagged as noisy and fewer than 10% of the independent components were removed during the cleaning process. Among these sections, we selected the one with the least amount of detected artifacts per minute of recording. Subsequently, we computed multi-electrode power spectra for the selected stationary section using a fast Fourier transform. Then, we fitted the power spectrum in the frequency range of 1–40 Hz to a CTM, as described above.

2.3.2. Personalized stimulus derivation

We can easily integrate external stimulation signals into each of the CTM populations by modifying $\mathbf{J}^{\star}\boldsymbol{\phi}^{\star}$ in equation (11). By representing the stimulations applied to the cortical excitatory population, cortical inhibitory population, thalamic reticular nucleus, and thalamic relay nuclei as the firing rates ϕ_x, ϕ_y, ϕ_z, and ϕ_w, respectively, we can express the CTM equations as equation (15)

$$\begin{bmatrix} D_e & 0 & 0 & 0 \\ 0 & D_i & 0 & 0 \\ 0 & 0 & D_r & 0 \\ 0 & 0 & 0 & D_s \end{bmatrix} \cdot \begin{bmatrix} \phi_e \\ \phi_i \\ \phi_r \\ \phi_s \end{bmatrix} = \begin{bmatrix} J_{ee} & J_{ei} & 0 & J_{es} \\ J_{ie} & J_{ii} & 0 & J_{is} \\ J_{re} & 0 & 0 & J_{rs} \\ J_{se} & 0 & J_{sr} & 0 \end{bmatrix} \cdot \begin{bmatrix} \phi_e \\ \phi_i \\ \phi_r \\ \phi_s \end{bmatrix} + \begin{bmatrix} J_{ex}\phi_x \\ J_{iy}\phi_y \\ J_{rz}\phi_z \\ J_{sw}\phi_w + J_{sn}\phi_n \end{bmatrix} \tag{15}$$

The solutions for the stimulation applied to each CTM population (separately) have a general form of:

$$\phi_e(\mathbf{k},\omega) = \left[C^{\text{stim}}(\omega)\,\phi^{\text{stim}}(\omega) + \phi_n(\omega)\right] \cdot \Psi(\mathbf{k},\omega) \tag{16}$$

$$P(\omega) = \left|C^{\text{stim}}(\omega)\,\phi^{\text{stim}}(\omega) + \phi_n(\omega)\right|^2 \cdot U(\omega) \tag{17}$$

when C^{stim} is a stimulus-dependent function derived from equation (15). CTM power spectra for different stimulation targets are presented in table 1.

In scenarios where a broad cortical region is stimulated, as is common in transcranial techniques such as rTMS or tACS, we assume that both the excitatory and inhibitory populations are excited concurrently by $\phi_{xy}(\omega)$. In this scenario, the power spectrum $P(\omega)$ can be expressed as follows:

$$P(\omega) = \left| \frac{\left(G_{ei}G_{iy} + \frac{G_{ex}}{L(\omega)} - G_{ei}G_{ex}\right)\left(1 - G_{srs}L^2(\omega)\right)}{G_{sn}G_{es}e^{i\omega t_0/2}}\phi_{xy}(\omega) + \phi_n(\omega) \right|^2 \cdot U(\omega) \tag{18}$$

It is important to note that both rTMS and tACS typically target specific brain networks rather than the entire cortex, focusing on regions such as the dorsolateral prefrontal cortex that have been observed to have a greater impact on DoC patients compared to

other areas [9, 20–22]. However, the CTM does not possess the multi-regional resolution required to simulate the cortex at this level of detail. Additionally, here, we do not consider potential variations in the response to TMS between inhibitory and excitatory populations. High-intensity stimulation primarily triggers firing in excitatory-to-excitatory axons due to their extensive spatial coverage and alignment with the electric field generated by TMS. In contrast, lower stimulation intensities are more likely to elicit firing events in inhibitory cells due to their lower firing thresholds [32].

2.3.3. Stimulus equations

As previously mentioned, to derive the stimulus formula, we need to solve $P^{\text{hlt}}(\omega) = P^{\text{doc+stim}}(\omega)$. Therefore, after fitting a CTM to a patient with DoC, we substitute $P^{\text{doc+stim}}(\omega)$ with equation (17), resulting in the following expression:

$$P^{\text{hlt}}(\omega) = \left|C^{\text{stim}}(\omega)\,\phi^{\text{stim}}(\omega) + \phi_n^{\text{doc}}(\omega)\right|^2 \cdot U^{\text{doc}}(\omega) \tag{19}$$

and

$$\frac{P^{\text{hlt}}(\omega)}{U^{\text{doc}}(\omega)} = \left||C^{\text{stim}}(\omega)|e^{i\angle C^{\text{stim}}(\omega)} \cdot |\phi^{\text{stim}}(\omega)|e^{i\angle\phi^{\text{stim}}(\omega)} + |\phi_n^{\text{doc}}(\omega)|e^{i\angle\phi_n^{\text{doc}}(\omega)}\right|^2 \tag{20}$$

To extract $|\phi^{\text{stim}}|$ in equation (20), we need to set $|\phi_n| = 1$, as previously mentioned. Additionally, we must determine the stimulus phase $\angle\phi^{\text{stim}}(\omega)$. Equation (13) provides information about the amplitude at each frequency, but does not impose constraints on the phase. Therefore, we allow ourselves to set the phase in a manner that is instrumental in solving the equation above. Specifically, we set it as a function of $\angle\phi_n^{\text{doc}}(\omega)$ and add π to introduce a negative sign in $C^{\text{stim}}(\omega)$, as shown in equation (21). For consistency with the theory, we set $\angle\phi_n^{\text{doc}}(\omega)$ to be a random number with a uniform distribution since ϕ_n is approximated by white Gaussian noise

$$\angle\phi^{\text{stim}}(\omega) = \angle\phi_n^{\text{doc}}(\omega) - \angle C^{\text{stim}}(\omega) - \pi \tag{21}$$

and get:

$$\frac{P^{\text{hlt}}(\omega)}{U^{\text{doc}}(\omega)} = \left|\left(-|C^{\text{stim}}(\omega)| \cdot |\phi^{\text{stim}}(\omega)| + 1\right)e^{i\angle\phi_n^{\text{doc}}(\omega)}\right|^2 \tag{22}$$

$$\left|\phi^{\text{stim}}(\omega)\right| = \frac{-1 \pm \sqrt{\frac{P^{\text{hlt}}(\omega)}{U^{\text{doc}}(\omega)}}}{-|C^{\text{stim}}(\omega)|} \tag{23}$$

To obtain a positive power spectrum, we opted for a negative sign before the square root in the expression. Additionally, we can set $U^{\text{doc}} = P^{\text{doc}}/|\phi_n^{\text{doc}}|^2 = P^{\text{doc}}$, while keeping in mind that $P^{\text{doc}}(\omega)$ is an analytical formula. It is important to note that unlike P^{hlt} that can be either analytical or experimental, $P^{\text{hlt}}_{\text{EXP}}$, $P^{\text{doc}}(\omega)$ cannot be experimental since there must be consistency between the power spectra and C^{stim}, which relies on fitted parameters

$$|\phi^{\text{stim}}(\omega)| = \frac{1 + \sqrt{\frac{P^{\text{hlt}}(\omega)}{P^{\text{doc}}(\omega)}}}{|C^{\text{stim}}(\omega)|} \tag{24}$$

By performing an inverse Fourier transform of $\phi^{\text{stim}}(\omega)$, we construct the stimulus time series $\phi^{\text{stim}}(t)$. Table 2 presents the amplitudes and the phases of stimuli applied to the various populations of the CTM.

At this point, we can also determine the stimulus intensity value for practical purposes, as outlined in the discussion section. This can be achieved by tuning G_{ex}, G_{iy}, G_{rz}, and G_{sw}, which were initially set to 1. However, it is worth noting that the value of G_{sn} was determined during the fitting process, as previously mentioned.

2.3.4. EEG signal generation

We generated artificial EEG signals from models with 'Healthy-fitted', 'DoC-fitted', and 'DoC-fitted with stimulation' parameter sets. These signals were generated for a duration of 30 s and were sampled at a rate of 125 Hz. Since the generated signal achieves stationarity after 5 s (which were disregarded), this duration proves adequate for computing power spectra. The EEG signals were simulated on a 0.5 m × 0.5 m square sheet, covering 784 locations. To make the simulated signals comparable to the experimental data, we interpolated them to match the locations of the 137 experimental electrodes and high-pass filtered those above 0.2 Hz.

2.3.5. Transient and long-lasting changes

Further, we investigated whether the constructed stimulus signal could induce a long-lasting change in the model's behavior, i.e. a bifurcation. We generated 150 s EEG signals from a model with a 'DoC-fitted' parameter set, while the stimulus was active between the 30th and 60th seconds. We computed the spectrogram of the Cz electrode signal and examined the time periods before, during, and after the stimulation.

However, while a CTM fitted to steady-state activity is generally stable, its susceptibility to perturbations may vary depending on the proximity of its

Table 1. CTM power spectra for different stimulation targets.

Stimulation Target Population	$P(\omega)$
Cortical excitatory C_x^{stim}, ϕ_x	$\left\lvert \frac{G_{ex}(1-G_{ei}L(\omega))(1-G_{srs}L^2(\omega))}{G_{sn}G_{es}L(\omega)e^{i\omega t_0/2}}\phi_x(\omega)+\phi_n(\omega)\right\rvert^2 \cdot U(\omega)$
Cortical inhibitory C_y^{stim}, ϕ_y	$\left\lvert \frac{G_{iy}G_{ei}(1-G_{srs}L^2(\omega))}{G_{sn}G_{es}e^{i\omega t_0/2}}\phi_y(\omega)+\phi_n(\omega)\right\rvert^2 \cdot U(\omega)$
Reticular nucleus C_z^{stim}, ϕ_z	$\left\lvert \frac{-\lvert G_{rz}\rvert G_{sr}L(\omega)}{G_{sn}}\phi_z(\omega)+\phi_n(\omega)\right\rvert^2 \cdot U(\omega)$
Relay nuclei C_w^{stim}, ϕ_w	$\left\lvert \frac{G_{sw}}{G_{sn}}\phi_w(\omega)+\phi_n(\omega)\right\rvert^2 \cdot U(\omega)$

Table 2. Stimuli amplitudes and phases.

Stimulus Target	Amplitude	Phase
Cortex $\phi_{xy}(\omega)$	$\left(1+\sqrt{\frac{P^{\text{hlt}}(\omega)}{P^{\text{doc}}(\omega)}}\right)\cdot \frac{G_{sn}G_{es}}{\left\lvert (G_{ei}G_{iy}+\frac{G_{ex}}{L(\omega)}-G_{ei}G_{ex})(1-G_{srs}L^2(\omega))\right\rvert}$	$\angle\phi_n^{\text{doc}}(\omega)+\omega t_0/2-\pi-\angle\left[(G_{ei}G_{iy}+\frac{G_{ex}}{L(\omega)}-G_{ei}G_{ex})(1-G_{srs}L^2(\omega))\right]$
Reticular nucleus $\phi_z(\omega)$	$\left(1+\sqrt{\frac{P^{\text{hlt}}(\omega)}{P^{\text{doc}}(\omega)}}\right)\cdot\frac{G_{sn}}{G_{rz}\lvert G_{sr}L(\omega)\rvert}$	$\angle\phi_n^{\text{doc}}(\omega)-\angle L(\omega)$
Relay nuclei $\phi_w(\omega)$	$\left(1+\sqrt{\frac{P^{\text{hlt}}(\omega)}{P^{\text{doc}}(\omega)}}\right)\cdot\frac{G_{sn}}{G_{sw}}$	$\angle\phi_n^{\text{doc}}(\omega)-\pi$

Amplitudes and the phases of $\phi^{\text{stim}}(\omega)$ applied to the different populations of the CTM. By performing an inverse Fourier transform, we get the time series $\phi^{\text{stim}}(t)$.

fitted parameters to the stability boundary. The stability of the CTM is determined by the denominator in equation (12). When all the zeros of equation (25) satisfy $\text{Im}(\omega_0) < 0$, the model is stable. Model stability boundaries can be represented in a three-dimensional space, as defined in equation (26). The X,Y,Z parameters correspond to corticocortical, corticothalamic, and intrathalamic loop strengths, respectively. These parameters offer a qualitative representation of the majority of CTM's dynamics and provide insights into its stability characteristics across various parameter values [28]. By adjusting these parameters, we can move the fitted model closer to the stability boundary, allowing it to alter its state in response to stimulation

$$\left(1-G_{srs}L^2\right)\left(1-G_{ei}L\right)\left(k^2r_e^2+q^2r_e^2\right)=0 \quad (25)$$

$$X=\frac{G_{ee}}{1-G_{ei}},\quad Y=G_{es}\frac{G_{se}+G_{sr}G_{re}}{(1-G_{srs})(1-G_{ei})},$$
$$Z=-G_{srs}\frac{\alpha\beta}{(\alpha+\beta)^2} \quad (26)$$

A notable stability region in the CTM is represented by the equation $X+Y<1$ [56]. When a model's fitted parameters are near this stability boundary (e.g. $X+Y=0.9$), external stimulation can induce a (saddle-node) bifurcation. However, in models positioned in a more stable zone (e.g. $X+Y=0.5$), introducing instability and triggering a bifurcation requires deliberately shifting the model to a critical point $X+Y=1$. This was achieved by setting the value of G_{ee} according to equation (27). It is important to note, however, that since G_{ee} also affects the power spectra (see equation (12)), this approach cannot be applied to a fitted model as it will cease to produce the desired spectrum.

In summary, when the base model is too stable, it cannot sustain any changes induced by the stimulus. As an alternative path, we chose to modify the fitted parameters (i.e. the parameters that determine the DoC power spectrum, effectively changing it to the representation of a different, virtual patient) to illustrate that under the right conditions (i.e. $X+Y=1$), our proposed method holds the potential to bring about lasting changes in a fitted CTM, regardless of its initial proximity to a stability boundary

$$G_{ee}^{\text{NEW}}=G_{ee}\frac{1-Y}{X} \quad (27)$$

3. Results

We successfully tested our methodology on subjects from the dataset. In the following results, we showcase its functionality using two pairs of DoC patients and healthy subjects. As evident from the calculations, the stimulus derivation procedure is nearly deterministic and can be applied to any pair of subjects with distinct power spectra, as we demonstrate further. It is important to note that the non-deterministic component, particularly ϕ_n^{doc}, introduces some white noise to the output, but it does not alter the spectral shape [57].

3.1. Power spectra

Figure 5 illustrates the outcomes of stimulation applied to the thalamic reticular nucleus of the MCS patient and to the cortex of the UWS patient, as expressed in the power spectra. We constructed a stimulus time series for different regions of CTMs fitted to these patients. Upon applying the stimulation to the models, we observed that the power spectra of the simulated EEG closely resembled those of

healthy subjects, exhibiting increased power at alpha and beta bands, characteristic of healthy individuals. This observation was further validated by computing the Pearson correlation coefficient between the power spectra values from 1 to 40 Hz at a 0.25 Hz resolution. In all cases, we observed a significant increase in the correlation coefficient from $R(P^{\text{hlt}}, P^{\text{doc}})$ to $R(P^{\text{hlt}}, P^{\text{doc+stim}})$. Notably, all the stimuli constructed for the other CTM populations induced the same power spectra as the spectra presented in figure 5. Additionally, we generated stimulations based on an experimental healthy spectrum (see figure 5(c)). Although $P^{\text{doc+stim}}_{\text{SIM}}$ did not match $P^{\text{hlt}}_{\text{EXP}}$ as closely as $P^{\text{hlt}}_{\text{SIM}}$, it still produced a satisfactory approximation. Overall, these outcomes highlight the efficacy of our approach in obtaining healthy-like EEG spectra in CTMs fitted to DoC patients.

It can be observed that while the experimental DoC and healthy EEG power spectra are entirely different (figure 5(c)), the fine details (small fluctuations) of the model-generated DoC and healthy spectra appear quite similar (figures 5(a) and (b)). This can be attributed to the EEG generation process, which involves fixed settings during the numerical solution of the model equations [31].

3.2. Phase constraints

In our experimental setup, the random number generator used for generating sensory inputs during model simulation was different from the one used for stimulus construction. This means that phase $\angle\phi_n^{\text{doc}}(\omega)$ used in the injected stimulus was different from phase $\angle\phi_n^{\text{doc:SIM}}$ that fed the simulator, even though both followed a uniform distribution. This setup resembles a stimulation configuration when the real-time brain signal phases are not accounted for by the stimulation equipment. However, it contradicts our method's specific requirement, which states that the stimulus phase $\angle\phi^{\text{stim}}(\omega)$ depends on the thalamic sensory input phase $\angle\phi_n^{\text{doc}}(\omega)$ (see equation (21)). Fulfilling this requirement is exceptionally challenging, especially *in vivo*, where measuring thalamic inputs in real-time poses significant difficulties. Yet, as long as the condition $P^{\text{hlt}}(\omega) \geqslant P^{\text{doc}}(\omega)$ (equation (19)) is met for every ω (see figure 5(a), for instance), this disparity does not significantly affect the results. To further prove this point we experimented with creating a stimulus with a linear phase instead of a random one, while keeping the sensory inputs as white noise. The stimulus time series appeared different (see figures 6(a) and (b)), but the resulting $P^{\text{doc+stim}}$ in figure 5(a) remained unchanged.

However, when there are values of ω for which $P^{\text{hlt}}(\omega) < P^{\text{doc}}(\omega)$, it becomes crucial to maintain the defined relationship between $\angle\phi_n^{\text{stim}}(\omega)$ and $\angle\phi_n^{\text{doc}}(\omega)$. As shown in equation (19), $C^{\text{stim}}(\omega)\phi^{\text{stim}}(\omega)$ is added to the DoC power spectrum. It can either increase or decrease the power at different frequencies based on its phase; for example, adding a phase of π radians is equivalent to multiplying the amplitude by -1. In our experimental setup, since $\angle\phi_n^{\text{doc}}(\omega) \neq \angle\phi_n^{\text{doc:SIM}}$, a power decrease does not occur at frequencies where $P^{\text{hlt}}(\omega) < P^{\text{doc}}(\omega)$. An example illustrating this behavior can be seen in figure 6(c), where we exchanged the roles of the healthy subject and the MCS patient (stimulating the healthy subject in the thalamic reticular nucleus) to create a scenario where this issue arises. In this case, $P^{\text{doc+stim}}$ followed P^{doc} instead of P^{hlt}, and the stimulation did not yield the desired effect. It was also reflected in the correlation coefficient, as $R(P^{\text{hlt}}, P^{\text{doc+stim}})$ remained low and similar to $R(P^{\text{hlt}}, P^{\text{doc}})$.

3.3. Hysteresis and bifurcating effects

Figure 7 illustrates the changes in the CTM-generated signal spectrum before, during, and after the stimulation. The stimulus was administered to the thalamic relay nuclei in models fitted to MCS and UWS patients from the 30th to the 60th second. Throughout the stimulation period, there was a substantial increase in power across all frequencies, reflecting $P^{\text{hlt}}(\omega) > P^{\text{doc}}(\omega)$. However, after stimulation offset, the MCS patient model exhibited a different response compared to the UWS patient model.

In figure 7(a), we observe that the model of the MCS patient underwent a bifurcation due to the stimulation, and the model's activity did not revert to its initial state upon termination of the stimulation. Instead, the model maintained power levels observed during the stimulation, which were significantly higher compared to the pre-stimulation period. The activity pattern in the spectrogram appeared to combine an increased version of the initial activity (mostly below 4 Hz) with non-physiological artifacts.

As for the model of the UWS patient, following the termination of the stimulus, the model exhibited a hysteresis effect that lasted for a 2 s transient period, presenting intermediate power values before returning to its pre-stimulation state. Hence, no long-term changes in the model's output were observed following the stimulation (see figure 7(b)).

Inspecting the models' proximity to the critical point $X + Y = 1$, we found that the MCS patient model was very close to this threshold, with $X_{\text{MCS}} + Y_{\text{MCS}} = 0.93$, whereas the UWS patient model exhibited greater stability, with $X_{\text{UWS}} + Y_{\text{UWS}} = 0.4$. To investigate the impact of criticality, we deliberately destabilized the UWS model, shifting it to the critical point by setting $X_{\text{UWS}} + Y_{\text{UWS}} = 1$. Under this condition, stimulation induced a similar effect to that observed in the MCS model, triggering a bifurcation and altering activity patterns even after the stimulation ended (see figure 7(c)). Interestingly, during the stimulation period, the spectrogram looked similar to the stable case, but with a notable decrease in overall power, particularly above 4 Hz. Moreover, similar to

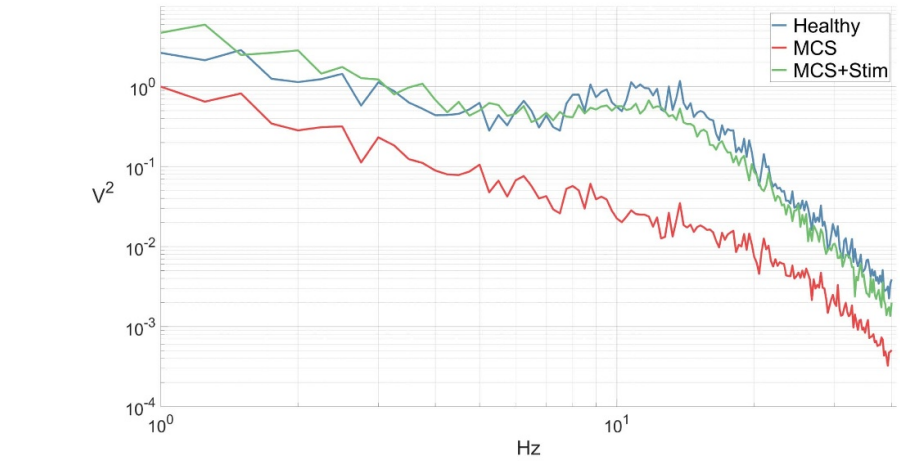

(a)

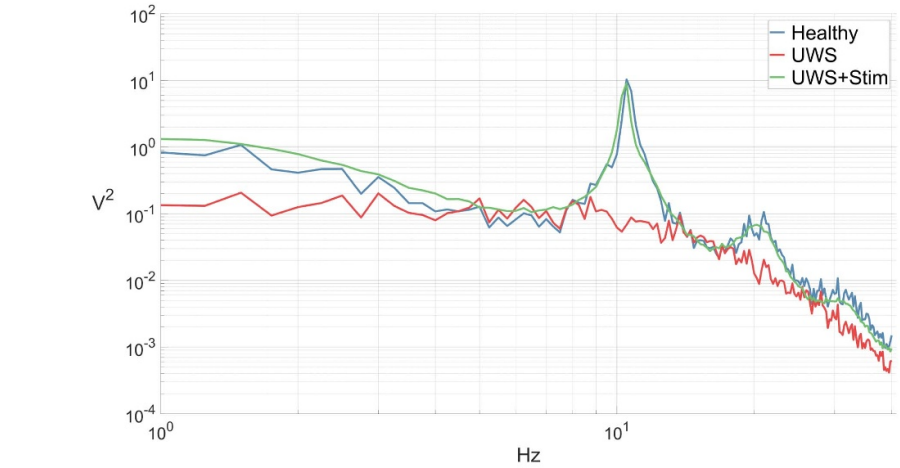

(b)

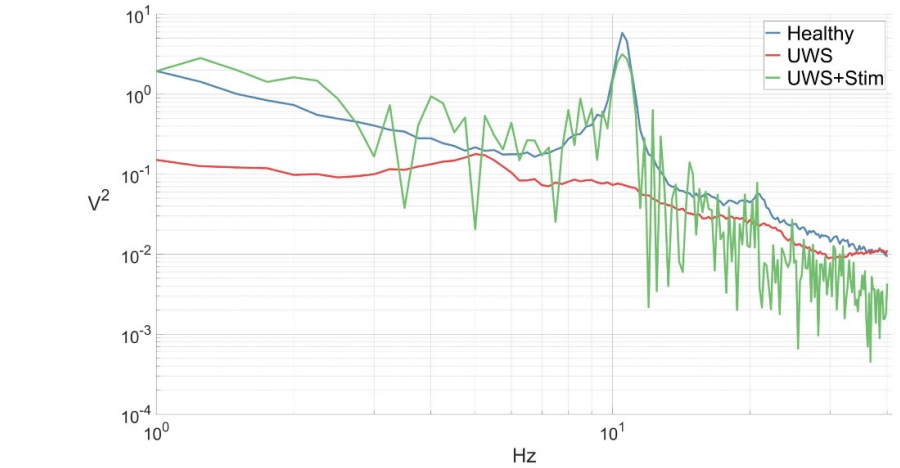

(c)

Figure 5. Power spectra comparison: examples of the stimulation on different patients and regions. The red curve represents the average power spectrum of a patient with DoC, the blue curve represents the average power spectrum of a healthy subject, and the green curve is the average power spectrum of a CTM-generated time series when the CTM is fitted to a patient with DoC and is stimulated in one of the CTM populations with the derived stimulus. (a) Minimally conscious state (MCS) patient and healthy subject #1: the stimulus is applied to the thalamic reticular nucleus. The stimulation significantly increased the correlation between the MCS and the healthy power spectra from $R(P^{\text{hlt}}, P^{\text{doc}}) = 0.519$ to $R(P^{\text{hlt}}, P^{\text{doc+stim}}) = 0.847$ ($p < 10^{-38}$). (b) Unresponsive wakefulness syndrome (UWS) patient and healthy subject #2: the stimulus is applied to the cortex. The stimulation significantly increased the correlation between the UWS and the healthy power spectra from $R(P^{\text{hlt}}, P^{\text{doc}}) = 0.205$ to $R(P^{\text{hlt}}, P^{\text{doc+stim}}) = 0.884$ ($p < 0.01$). (c) Same as *b*, but the red and blue curves are experimental EEG spectra, and $P^{\text{hlt}}_{\text{EXP}}(\omega)$ is used in the stimulus calculations. The stimulation significantly increased the correlation between the UWS and the healthy power spectra from $R(P^{\text{hlt}}, P^{\text{doc}}) = 0.355$ to $R(P^{\text{hlt}}, P^{\text{doc+stim}}) = 0.726$ ($p < 10^{-5}$).

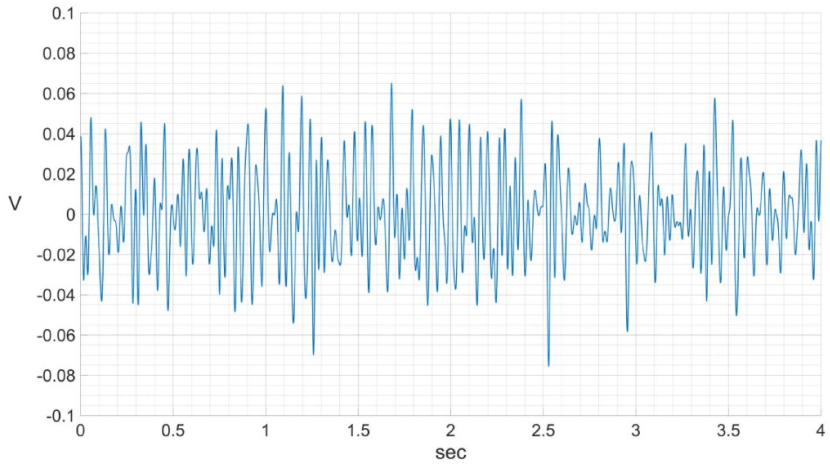

(a)

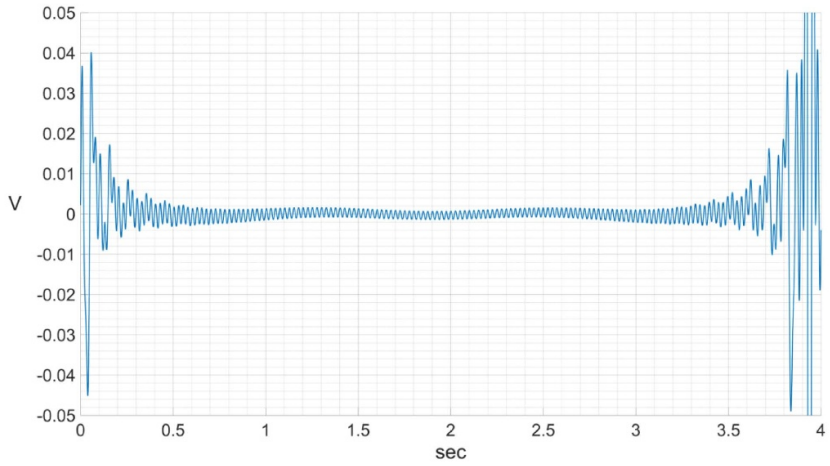

(b)

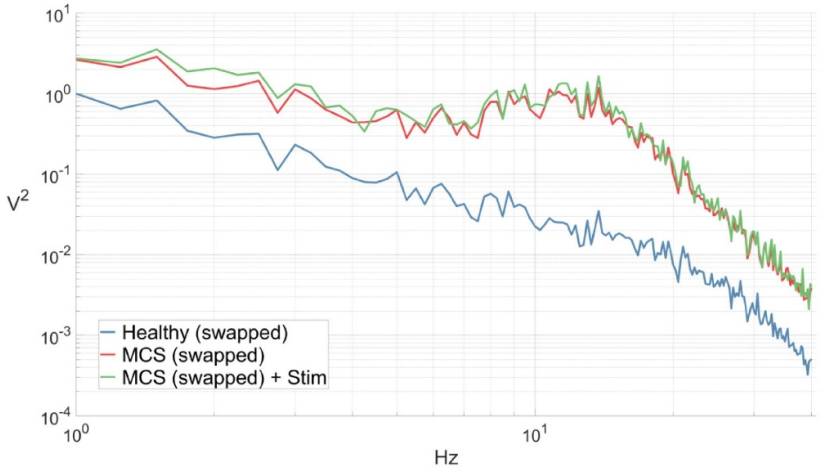

(c)

Figure 6. Stimulus phase effects. (a) and (b): Time series of the stimulus applied to the reticular nucleus, constructed for the MCS patient and healthy subject #1. The stimulus was calculated using $\phi_n^{\mathrm{doc}}(\omega)$ with a random phase (a) and a linear phase (b). Despite phase variations, the resulting signal power spectra remained consistent with figure 5(a). In (c), we swapped between healthy subject #1 and the MCS patient before stimulus construction to demonstrate that for $P^{\mathrm{hlt}}(\omega) < P^{\mathrm{doc}}(\omega)$, the stimulation fails due to a phase mismatch in the experimental setup. Consequently, the increase in correlation between the MCS and healthy power spectra post-stimulation was minimal: from $R(P^{\mathrm{hlt}}, P^{\mathrm{doc}}) = 0.519$ to $R(P^{\mathrm{hlt}}, P^{\mathrm{doc+stim}}) = 0.532$ ($p < 10^{-38}$).

the MCS model, activity below 4 Hz remained elevated after stimulus offset. This phenomenon may be explained by the CTM's tendency to exhibit critical slowing down near $X + Y = 1$ [56, 58, 59].

3.4. Method generality

Additionally, to demonstrate the generality of our method, we tested it on a pair of healthy subjects. As shown in figure 8 and supported by the correlation coefficient, applying a tailored stimulus to healthy subject #4 induced a power spectrum similar to that of subject #3. The stimulation was constructed and applied to the thalamic relay nuclei, but as observed in previous cases, applying the method to other CTM populations yielded identical power spectra to those presented here.

4. Discussion

Our study introduces a computational approach aimed at generating a signal capable of inducing healthy-like power spectra in patients with DoC. This involves fitting a CTM to the power spectrum of a patient with DoC and then utilizing the power spectrum of a healthy subject to derive a personalized stimulus time series. We applied our method to two patients with DoC, targeting brain regions commonly addressed in DBS, rTMS, and tACS. Consequently, these stimuli drove the CTM to generate EEG power spectra resembling those seen in healthy brains.

4.1. Potential, challenges and limitations

4.1.1. Clinical feasibility

A central question arises: Will this method be effective *in vivo*? As highlighted in the introduction, various brain stimulation therapies have been employed in the treatment of DoC, but their success has been only partial [9]. Our stimulus construction technique, once integrated into these therapies, aims to enhance their outcomes by inducing brain activity in patients that closely resembles the patterns seen in healthy individuals. This is grounded in two key assumptions that warrant further examination:

- The proposed model has the capacity to capture the brain dynamics of DoC patients and healthy individuals. In other words, once we apply this stimulation method to a real brain, it will yield an activity akin to the one produced by the model. If not, we may need to consider employing a model that is more complex, as detailed below.
- A healthy-like spectrum increases the likelihood of regaining consciousness. While this is both a philosophical and phenomenological query, the assumption is based on the research of neural correlates of consciousness [60–64]. Numerous studies have demonstrated significant differences in the power spectra of DoC patients compared to healthy controls [65–68]. While a state of consciousness frequently results in a power spectrum akin to that of a healthy individual, the opposite is not always true, and other factors might also be important (e.g. integration and segregation [69]).

Nevertheless, even if the above assumptions hold, this method requires thorough clinical validation before it can be used routinely. Numerous factors could lead to failure *in vivo*, ranging from suboptimal calibration to unknown physiological variables. Modeling all the structural and dynamical aspects of a healthy and pathological brain is inherently challenging, and there is always the risk of overlooking key elements. While NFT has demonstrated success across a wide range of phenomena, datasets, and stimulation modeling in previous studies [27–29, 32, 34, 41–47], there remains the possibility that it may not be effective in this particular application. It may even fail at fundamental steps, such as the spectrum fitting process, resulting in unstable or physiologically implausible solutions or yielding only a coarse fit that overlooks critical spectral features [28].

4.1.2. Plasticity and sustained changes

We propose that, beyond improving activity during stimulation, our personalized stimulation method, when used consistently over multiple sessions, may lead to longer-lasting effects compared to current stimulation approaches. We hypothesize that this method could more effectively engage the brain's natural plasticity mechanisms by inducing activity patterns similar to those observed in a healthy brain. Such activation could potentially aid in the brain's gradual recovery, helping it regain normal function without the continuous need for external intervention.

It has been demonstrated that intervention therapies, including brain stimulation, cognitive training, physical activity, and pharmaceutical treatments, can trigger plasticity mechanisms that facilitate recovery in DoC patients and other conditions requiring neural rehabilitation. The distinctiveness of our method, compared to other brain stimulation approaches, lies in its ability to induce healthy-like brain activity. This could further promote recovery by better engaging two key plasticity mechanisms: use-dependent plasticity and homeostatic plasticity [10, 70, 71].

Use-dependent plasticity refers to the strengthening or weakening of neural connections based on the recurrence and pattern of their activation. It is closely tied to long-term potentiation (and

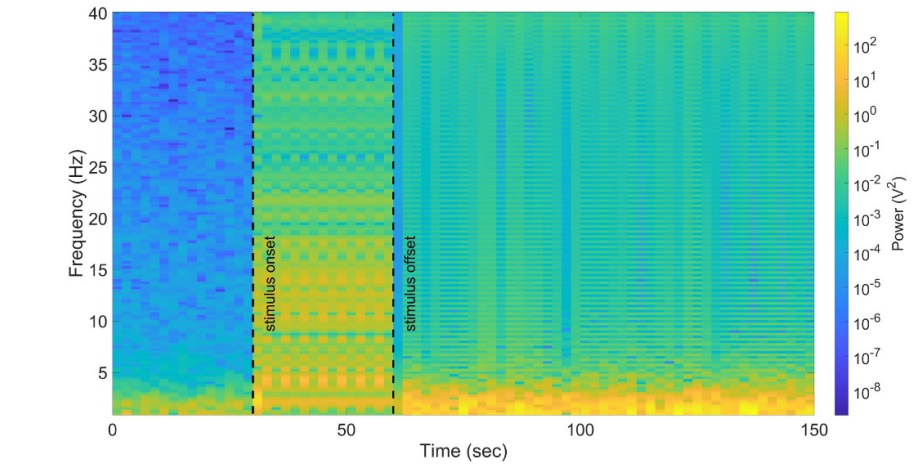

(a)

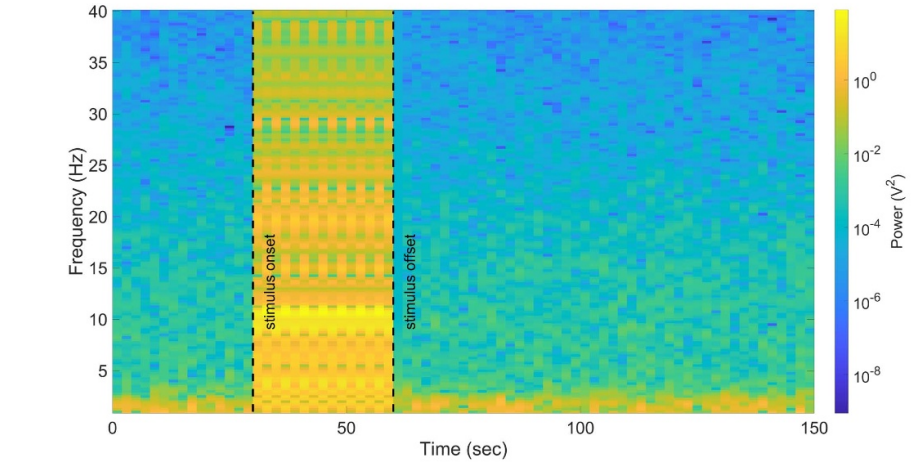

(b)

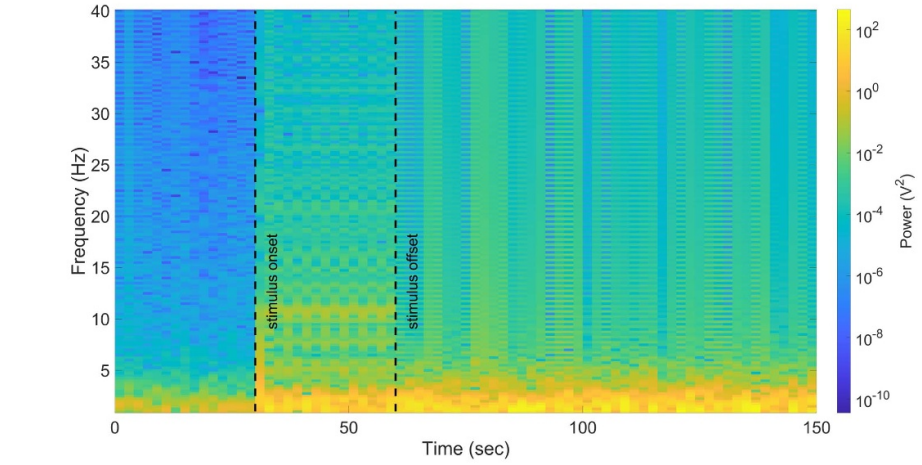

(c)

Figure 7. Transient and long-lasting changes. A 150 s spectrogram of a Cz electrode EEG time series generated from CTMs fitted to MCS and UWS patients. The models were stimulated in the thalamic relay nuclei from the 30th to the 60th second. (a) MCS patient model ($X_{\mathrm{MCS}} + Y_{\mathrm{MCS}} = 0.93$), stimulated using $P^{\mathrm{hlt}}_{\mathrm{EXP}}(\omega)$ from healthy subject #1. A sustained change in activity is observed post-stimulation. (b) UWS patient model ($X_{\mathrm{UWS}} + Y_{\mathrm{UWS}} = 0.4$), stimulated using $P^{\mathrm{hlt}}_{\mathrm{EXP}}(\omega)$ from healthy subject #2. Activity returns to baseline after a 2 s transient period. (c) Same as (b), but with the CTM brought to the critical point ($X_{\mathrm{UWS}} + Y_{\mathrm{UWS}} = 1$) before stimulation. A sustained change in activity is observed, similar to (a).

long-term depression) of synaptic strength, which is a fundamental mechanism underlying learning and memory. Repeated induction of the desired healthy activity in the brain can reinforce synaptic pathways, potentially sustaining and stabilizing the activity over time [10, 72, 73]. A clear example

Figure 8. Power spectra comparison: two healthy subjects. The blue curve represents the average power spectrum of healthy subject #3, the red curve represents the average power spectrum of healthy subject #4, and the green curve shows the average power spectrum of a CTM-generated time series when the CTM is fitted to subject #4 and stimulated at the thalamic relay nuclei. The stimulation significantly increased the correlation between healthy #3 and the healthy #4 power spectra from $R(P^{\text{hlt}_3}, P^{\text{hlt}_4}) = 0.888$ to $R(P^{\text{hlt}_3}, P^{\text{hlt}_4+\text{stim}}) = 0.956$ ($p < 10^{-53}$).

of this process occurs during motor recovery in stroke patients, where a paralyzed limb can regain mobility through repeated externally induced movements. Combining such physiotherapy with TMS has been shown to enhance recovery by desynchronizing pathological spike-timing-dependent plasticity and promoting long-term potentiation [8, 10, 74]. In our approach, brain stimulation not only desynchronizes pathological neural activity but also induces patterns of healthy brain activity, activating and directing use-dependent plasticity toward the desired outcome.

Homeostatic plasticity is a regulatory mechanism that stabilizes neural activity by adjusting synaptic strengths or intrinsic excitability [75]. For instance, normal sleep-wake cycles play a key role in stabilizing synaptic weights [76]. In contrast, in conditions such as DoC, inactive networks often exhibit pathological plasticity due to abnormal synaptic strength, which can lead to epileptic activity. Brain stimulation helps restore homeostatic plasticity by suppressing epileptic activity and re-establishing firing rate homeostasis. Additionally, simulations have demonstrated that when a previously inactive network is re-engaged, healthy brain activity helps normalize homeostatic plasticity. In particular, excitatory corticothalamic activity has been shown to support this recovery process [76–78]. Our approach integrates these principles by restoring homeostatic plasticity through stimulation, which enhances excitatory corticothalamic activity (as reflected in the elevated power spectra in figure 5) and regulates NFT firing rates $\phi(\mathbf{r}, t)$ to induce healthy-like activity.

Modeling these plasticity mechanisms requires incorporating time-dependent functions into model parameters and applying specific learning rules to adjust them, as demonstrated in prior studies [32, 76, 78, 79]. Nonetheless, even in the current model, which does not support neural plasticity, our results show that stimulation can induce long-lasting effects. When the CTM is near (or at) a stability boundary, the stimulation triggers a bifurcation, leading to substantial and persistent changes in the generated signal after stimulation offset. This aligns with previous studies suggesting that neuromodulation can alter the brain's proximity to criticality and even push it beyond a critical point [80]. While these changes differ significantly from the desired healthy-like activity, a more complex model could exhibit bifurcations that lead to the desired sustained activity when subjected to the constructed stimulation [58].

A deeper analysis of CTM dynamics is necessary to fully understand stimulation effects, particularly by examining trajectories within the XYZ parameter space (see equation (26)) [27, 81]. Such analysis could also help determine the $X + Y$ threshold, beyond which modifications to G_{ee} would be necessary to induce a bifurcation. Given all that, it is important to clarify that the limitation of the current model to present long-lasting effects does not negate the potential for such effects in our approach *in vivo*.

4.1.3. Increasing model complexity

As previously mentioned, it may be necessary to use a more intricate model to refine the stimulation and control its effects, thus improving the chances of success of this method in an *in-vivo* setting. The CTM, while capable of replicating various brain states and phenomena effectively, is inherently simplistic [26]. A more sophisticated model has the potential to offer a more accurate representation of both DoC and

healthy brains in terms of the desired bifurcations and neural plasticity. For instance, whereas the CTM is adequate for modeling typical sleep stages and wakefulness, unconventional arousal conditions like jet lag or caffeine intake necessitate the incorporation of additional dynamics and bifurcations. This can be achieved by establishing connections between the brainstem and hypothalamus with the CTM to drive transitions between different states, as demonstrated by Phillips *et al* [44, 58].

Furthermore, integrating additional brain regions into the CTM and enhancing the model resolution by subdividing its components would expand the scope of modeled stimulation techniques, facilitate targeted stimulation modeling, and potentially streamline the application of such stimulations more effectively. Specifically, incorporating the vagus nerve and the brainstem into the CTM would enable support for VNS. Segmenting the cortex into multiple populations would aid in modeling focused stimulation of specific brain networks as commonly practiced in rTMS and tACS. With detailed network modeling, which may encompass multiple cortical areas, various nuclei and ganglia (as in the case of a stimulation model for Parkinson's disease [34]), the most effective stimulation sites can be accurately identified, thereby guiding the placement of electrodes for a targeted DBS, or instead opting to apply a wide-angle rTMS [9, 11, 20]. Additionally, it allows for the simultaneous stimulation of different brain areas and for exploration of how stimuli propagate through the brain.

Another important motivation is related to the etiology of the DoC state. DoC can arise from diverse causes such as traumatic brain injury, anoxia/hypoxia, ischemic/hemorrhagic stroke, intoxication, and more [1]. Consequently, each DoC patient may present with a distinct etiology characterized by brain lesions, disrupted structural and functional connectivity, spatial variations in the cortex, and other factors. Given that stimulation is typically applied to healthy brain regions [82], modeling these specific pathologies is essential to tailor patient-specific stimulation.

Finally, to integrate our stimulus-derivation method into brain stimulation therapies like DBS or tACS, we must provide a model for them. This is necessary because these therapies involve constructing and transmitting stimuli in the form of electric currents or magnetic fields, whereas in our method the applied stimulus is represented as a firing rate $\phi^{\text{stim}}(t)$. The model needs to encompass parameters for constructing the signal for different stimulation protocols, modulatory effects of the mediums it propagates through, its influence on the neural activity of the target population (i.e. its translation to $\phi^{\text{stim}}(t)$), and additional side effects like tissue heating that may impact subsequent stimuli signals. Constructing such a model is possible within the NFT framework, as partially demonstrated in previous studies for DBS and rTMS [32, 34]. Such a model can also be created for non-electromagnetic therapies like low-intensity focused ultrasound pulsation, recently used as a therapy for DoC [6, 7, 83].

4.1.4. Sample size of participants

This study serves as a proof-of-concept for a novel method of personalized stimulus signal construction. We introduced its deterministic mathematical foundation and tested it on two DoC patients and four healthy subjects. However, the CTM is a complex dynamical system with multiple instabilities (besides $X+Y$). CTMs with individually fitted parameters, when subjected to various perturbations, may exhibit unexpected behaviors across different patients [27, 28, 56]. Therefore, to ensure robustness, enhance statistical power, and refine modeling constraints, further testing on a larger cohort is essential.

Additionally, testing more patients is necessary to determine how the stimulation effects vary across different DoC states. Here we already evidenced that stimulation in an MCS patient model triggered a bifurcation, whereas the UWS patient model required destabilization to achieve a similar effect (see figure 7). However, previous studies suggest that no single NFT parameter, including individual or combined *XYZ* values, reliably distinguishes between UWS and MCS states [29, 30]. Conversely, it was challenging to determine whether the spectral correlation results were significantly different between the two DoC states. Thus, further research with additional subjects is needed to investigate these aspects in greater detail.

4.2. Practical adaptations for *in-vivo* application

4.2.1. Integration with brain stimulation therapies

We plan to incorporate our stimulation approach into DBS, rTMS, and tACS brain stimulation therapies, however, as mentioned above, we first need to develop models for them. Then, we can invert these models to determine the stimulation protocols and their parameters based on $\phi^{\text{stim}}(t)$. The precise mechanisms underlying the effects of these stimulation modalities on neurons are still under investigation [19, 84, 85]. However, we can broadly model DBS and rTMS as spike-like signals with a firing rate of $Fr(t) = \phi^{\text{stim}}(t)$ and tACS as an electric potential $V(t) = \phi^{\text{stim}}(t)$. Consequently, in DBS and rTMS, ϕ^{stim} modulates the stimulation frequency (akin to an FM radio) through the alteration of inter-pulse intervals, whereas in tACS, it directly determines the signal.

The configuration of the stimulation parameters should be based on both $\phi^{\text{stim}}(t)$ and clinical requirements. Fine-tuning the stimulation power and frequency to align with individual patient needs and specific medical conditions is a standard practice in brain stimulation therapies, aimed at optimizing treatment outcomes, while minimizing adverse effects [86–89]. In the proposed models, the chosen stimulation frequency in DBS and rTMS (the 'carrier' frequency), and the direct voltage amplitude in tACS correspond to the average intensity of ϕ^{stim}, regulated by G_{ex}, G_{iy}, G_{rz}, and G_{sw}. However, as outlined in the methods section, the stimulus intensity is predetermined and should be set according to therapy properties, rather than vice versa. Therefore, we utilize the tuned stimulation power and frequency to determine the values of G_{ex}, G_{iy}, G_{rz}, and G_{sw}.

A potential protocol for integrating our method into DBS or rTMS therapies in a clinical setting would involve the following steps:

1. Compute the stimulus signal $\phi^{\text{stim}}(t)$ as described under 'Stimulus construction workflow' in the methods section.
2. Set up the stimulation therapy following standard clinical procedures. Adjust stimulation parameters and the stimulation ('carrier') frequency F_c in particular, based on the patient's condition and needs.
3. Calculate the intensity factor $B = \frac{F_c}{\langle \phi^{\text{stim}}(t) \rangle}$. This step is equivalent to determining G_{ex}, G_{iy}, G_{rz}, and G_{sw} (using the equations in table 2).
4. Modulate the stimulation frequency according to $F(t) = B \cdot \phi^{\text{stim}}(t)$.

For tACS therapy, the protocol is similar, but the adjusted parameter is the direct voltage amplitude V_0 instead of F_c. Thus, the transmitted stimulation signal is given by: $V(t) = B \cdot \phi^{\text{stim}}(t) = \frac{V_0}{\langle \phi^{\text{stim}}(t) \rangle} \phi^{\text{stim}}(t)$.

4.2.2. Sensory input phase acquisition

As outlined in equation (21), the thalamic sensory input phase $\angle \phi_n^{\text{doc}}(\omega)$ is necessary for the calculation of ϕ^{stim}. We demonstrated that when $P^{\text{hlt}}(\omega) \geqslant P^{\text{doc}}(\omega)$, it is possible to set any arbitrary phase instead of $\angle \phi_n^{\text{doc}}(\omega)$ during the stimulus calculation. However, when this condition is not met, precise knowledge of the sensory input phase becomes crucial.

Theoretically, acquiring the sensory input phase would require measuring the activity of all the thalamic afferent neurons, which is not feasible with present technology. Nonetheless, strides have been made in this direction, such as estimating the phase from population activity and synchronizing DBS signals with neural activity for more efficient Parkinson's disease treatment [90]. Alternatively, selecting a high-power P^{hlt} could circumvent this obstacle.

4.2.3. Closed-loop stimulation

Our method can be combined with closed-loop stimulation, a paradigm for personalizing neuromodulation that has made a lot of progress in recent years. Grounded in control theory, closed-loop brain stimulation involves the continuous monitoring of brain activity, providing real-time feedback to adjust stimulation parameters. This approach has significantly improved therapies like DBS, rTMS, and tDCS, enhancing response rates and reducing outcome variability for conditions such as Parkinson's disease, epilepsy, depression, and DoC [83, 91–93].

In our method, real-time closed-loop feedback can maintain the patient's power spectrum at the desired level during stimulation. Any deviations will dynamically adjust the intensity of ϕ^{stim} through the parameters G_{ex}, G_{iy}, G_{rz}, and G_{sw}. These adjustments, in turn, will regulate the 'carrier' frequency or the direct voltage amplitude, depending on the specific stimulation therapy used.

In order to fully adapt the stimulus for real-time closed-loop feedback, the model parameters need to exhibit temporal variability, i.e. representing plasticity effects. Without this adaptation, our current stimulus construction method does not allow parameters to be updated in real-time during stimulation, as the available feedback biomarker is the resting-state EEG spectrum, obtained when stimulation is off, possible only between therapy sessions. Temporal variability in parameters will transform the power spectrum into a dynamic equation that integrates feedback inputs. This also suggests that real-time closed-loop feedback will enhance the performance of models incorporating plasticity compared to periodic updates every few minutes.

4.2.4. Brain–computer interface paradigms

A promising way to enhance the proposed stimulation method is by incorporating brain–computer interface (BCI) paradigms. BCIs capture and interpret neural activity while users engage in specific tasks, enabling control over external devices and artificial limbs, or communicate non-verbally. Common EEG-based BCI paradigms, such as P300 or motor imagery, have proven effective in diagnosing and assessing the prognosis of DoC by measuring patient communication and engagement with their environment [94–96]. Performance metrics from these paradigms can be used to evaluate awareness and covert responsiveness during and after stimulation, providing real-time feedback for adjusting stimulation parameters in a closed-loop system. This integration also provides a framework for tracking long-term progress and ultimately improving

the prognosis for DoC patients [97]. Furthermore, BCI-based neurofeedback training can complement our stimulation method as a rehabilitation strategy, helping patients gradually regain voluntary control over brain activity and enhancing neuroplasticity-driven recovery. A similar approach has demonstrated substantial success in motor rehabilitation for stroke patients, where motor imagery training combined with functional electrical stimulation significantly improved motor function [98]. Finally, NFT has previously been applied to enhance motor imagery, further supporting the feasibility of combining the proposed stimulation method with BCI [99].

4.3. Further applications and extensions

As we previously mentioned, our proposed approach offers versatility and can be adapted to various spectra and applied to different brain regions modeled by NFT. It is evident from the calculations of the stimulus derivation, that they can be applied to any two individuals, regardless of their medical condition. Essentially, with the EEG power spectra of two individuals, we can construct a stimulus signal that will cause person #1 to induce the power spectrum of person #2, for as long as the stimulus is applied, as demonstrated in figure 8. The only constraint is imposed by the availability of a sensory input phase, required for cases when $P^{\#2}(\omega) < P^{\#1}(\omega)$. Moreover, NFT models can be fitted to power spectra acquired through other neuroimaging techniques such as magnetoencephalography and intracranial electroencephalography, in addition to electroencephalography [26]. Therefore, the potential application of our method extends beyond DoC, making it suitable for addressing a broad range of medical conditions across diverse imaging and stimulation settings.

Furthermore, as stated above, the model can be expanded by incorporating additional brain regions and stimulating them as desired [34]. For instance, we can create personalized stimuli for DBS treatment for depression, where remission rates are just above 50%. This extension would involve modeling the limbic system and stimulating regions like the striatum and subgenual cingulate cortex. Although the equations will differ, the core approach remains consistent, with the use of $P^{\text{depression}}$ in place of P^{doc}. Our method has significant potential to improve treatment outcomes by enhancing the longevity of therapeutic effects and aiding in target selection [100, 101].

Finally, it would be intriguing to investigate whether, by toggling between P^{hlt} and P^{doc} (and accounting for sensory input phase $\angle\phi_n^{\text{doc}}(\omega)$), one could induce a reversible anesthesia-like state in a healthy subject. This exploration could shed light on the potential for this method to modulate brain activity across various physiological and altered states.

5. Summary

In this research, we introduced a novel computational method aimed at modulating brain activity in patients with DoC. Our approach focused on constructing a stimulus signal that could induce a healthy-like neural activity pattern in these patients. To achieve this, we utilized a simplified brain model based on NFT and adapted it to reproduce the power spectrum of DoC patients. The core idea of our method involved fitting this NFT model to the power spectrum of the patients and, subsequently, using the power spectrum of healthy subjects to derive stimulus time series. By applying the derived signal to brain regions typically targeted by therapies like DBS, rTMS, and tACS, we demonstrated that our stimuli induced EEG power spectra resembling those of healthy individuals. We speculate that once the brain produces a healthy-like activity, both use-dependent and homeostatic plasticity mechanisms are triggered, potentially leading to long-lasting changes and improvement in a patient's consciousness level compared to current stimulation approaches.

While our results provide promising insights into the potential of this approach, several critical considerations and avenues for future exploration should be noted. Firstly, the development of various stimulation therapy models needs to be pursued and integrated with the proposed NFT model to bridge the gap between theoretical frameworks and practical applications. Moreover, the implementation of our method in clinical settings requires comprehensive validation and a thorough comparison with the outcomes of existing stimulation protocols to ensure its efficacy and safety. Key questions include whether the computational model accurately represents the complexity of the DoC brain and whether the assumption that a healthy-like power spectrum implies consciousness holds true *in vivo*.

Additionally, we discussed the importance of testing more complex models to capture the intricate nature of DoC and to enable targeted stimulation. Detailed models could help determine optimal stimulation locations and patterns, thereby enhancing the efficacy of brain stimulation therapies. Furthermore, understanding the specific etiology of DoC in an individual patient and modeling those associated pathologies may be crucial for personalized stimulation strategies.

It is important to emphasize the generalizability of our stimulus derivation technique, as its computations are deterministic and adaptable to any pair of subjects with different power spectra. The only constraint in certain cases is the availability of sensory phase information. Therefore, this technique can be tailored to address other pathologies treated with

brain stimulation beyond DoC, opening up a multitude of potential avenues for exploration.

In conclusion, our research provides a proof-of-concept computational framework for designing patient-specific brain stimulation therapies. While further research specifically aiming at clinical translation is needed, this method holds promise for improving the outcomes of future neuromodulation therapies for DoC patients and could be extended to treat other conditions amenable to brain stimulation interventions.

Data availability statement

The data that support the findings of this study are openly available at the following URL/DOI: https://zenodo.org/records/11212096.

Acknowledgments

We would like to thank Avigail Makbili from the Computational Psychiatry Lab at Ben-Gurion University, who took part in the processing and cleaning of the experimental EEG data. Additionally, we want to thank Prof. Yaniv Zigel from the Department of Biomedical Engineering at Ben-Gurion University, who helped develop the mathematics of this method.

Funding for this work was provided by a grant from the EU CHIST-ERA program. Additionally, this work was supported by the University and University Hospital of Liège, the Belgian National Funds for Scientific Research (FRS-FNRS), the FNRS PDR Project (T.0134.21), the ERA-Net FLAG-ERA JTC2021 Project ModelDXConsciousness (the Human Brain Project Partnering Project), the DoC-Box project (HORIZON-MSCA-2022-SE-01-01-101131344), and the FNRS MIS Project (F.4521.23), JA is postdoctoral fellow funded (1265522N) by the Fund for Scientific Research-Flanders (FWO), OG is a research associate at FRS-FNRS.

The wording revision process of this article included the use of ChatGPT by OpenAI.

Each author contributed to this work as follows: DP conceptualized and led the project, developed the methodology and part of the software, analyzed, investigated, and validated the results, created the figures, wrote and edited the manuscript; PR: developed the methodology, reviewed and edited the manuscript; EM: developed part of the software, reviewed and edited the manuscript; GVDL: reviewed and edited the manuscript; PN: reviewed and edited the manuscript; JA: acquired the data, reviewed and edited the manuscript; OG: acquired the data, acquired funding, reviewed and edited the manuscript; OS: conceptualized and supervised the project, acquired funding, reviewed and edited the manuscript.

ORCID iDs

Daniel Polyakov https://orcid.org/0000-0001-5768-3373
P A Robinson https://orcid.org/0000-0003-4100-6049
Eli J Müller https://orcid.org/0000-0003-2497-0194
Glenn van der Lande https://orcid.org/0000-0003-0518-2571
Pablo Núñez https://orcid.org/0000-0002-5898-6664
Jitka Annen https://orcid.org/0000-0002-7459-4345
Olivia Gosseries https://orcid.org/0000-0001-9011-7496
Oren Shriki https://orcid.org/0000-0003-1129-4799

References

[1] Bernat J L 2006 Chronic disorders of consciousness *Lancet Neurol.* **367** 1181–92
[2] Gosseries O, Bruno M-A, Chatelle C, Vanhaudenhuyse A, Schnakers C, Soddu A and Laureys S 2011 Disorders of consciousness: what's in a name? *NeuroRehabilitation* **28** 3–14
[3] Giacino J T, Kalmar K and Whyte J 2004 The JFK Coma Recovery Scale-Revised: measurement characteristics and diagnostic utility *Arch. Phys. Med. Rehabil.* **85** 2020–9
[4] Annen J *et al* 2019 Diagnostic accuracy of the CRS-R index in patients with disorders of consciousness *Brain Inj.* **33** 1409–12
[5] Thibaut A, Schiff N, Giacino J, Laureys S and Gosseries O 2019 Therapeutic interventions in patients with prolonged disorders of consciousness *Lancet Neurol.* **18** 600–14
[6] Shou Z, Li Z, Wang X, Chen M, Bai Y and Di H 2021 Non-invasive brain intervention techniques used in patients with disorders of consciousness *Int. J. Neurosci.* **131** 390–404
[7] Edlow B L *et al* 2021 Therapies to restore consciousness in patients with severe brain injuries: a gap analysis and future directions *Neurocritical Care* **35** 68–85
[8] Mawase F, Uehara S, Bastian A J and Celnik P 2017 Motor learning enhances use-dependent plasticity *J. Neurosci.* **37** 2673–85
[9] Bourdillon P, Hermann B, Sitt J D and Naccache L 2019 Electromagnetic brain stimulation in patients with disorders of consciousness *Front. Neurosci.* **13** 1–14
[10] Kumar J *et al* 2023 Innovative approaches and therapies to enhance neuroplasticity and promote recovery in patients with neurological disorders: a narrative review *Cureus* **15** e41914
[11] van der Lande G J M *et al* 2024 Brain state identification and neuromodulation to promote recovery of consciousness *Brain Commun.* **6** 1–50
[12] Yamamoto T, Katayama Y, Kobayashi K, Oshima H, Fukaya C and Tsubokawa T 2010 Deep brain stimulation for the treatment of vegetative state *Eur. J. Neurosci.* **32** 1145–51
[13] Magrassi L, Maggioni G, Pistarini C, Di Perri C, Bastianello S, Zippo A G, Iotti G A, Biella G E M and Imberti R 2016 Results of a prospective study (CATS) on the effects of thalamic stimulation in minimally conscious and vegetative state patients *J. Neurosurg.* **125** 972–81

[14] Chudy D, Deletis V, Almahariq F, Marčinković P, Škrlin J and Physioth B 2018 Deep brain stimulation for the early treatment of the minimally conscious state and vegetative state: experience in 14 patients *J. Neurosurg.* **128** 1189–98
[15] Cao T *et al* 2023 Clinical neuromodulatory effects of deep brain stimulation in disorder of consciousness: a literature review *CNS Neurosci. Ther.* **30** 1–17
[16] Wu Y *et al* 2023 Spinal cord stimulation and deep brain stimulation for disorders of consciousness: a systematic review and individual patient data analysis of 608 cases *Neurosurg. Rev.* **46** 1–13
[17] Yuan H and Silberstein S D 2016 Vagus nerve and vagus nerve stimulation, a comprehensive review: part II *Headache* **56** 259–66
[18] Xiang X J *et al* 2020 The clinical effect of vagus nerve stimulation in the treatment of patients with a minimally conscious state *J. Neurorestoratol.* **8** 160–71
[19] Rajan T S, Ghilardi M F M, Wang H-Y, Mazzon E, Bramanti P, Restivo D and Quartarone A 2017 Mechanism of action for rTMS: a working hypothesis based on animal studies *Front. Physiol.* **8** 1–3
[20] Yang Z *et al* 2023 Behavioral effects of repetitive transcranial magnetic stimulation in disorders of consciousness: a systematic review and meta-analysis *Brain Sci.* **13** 1362
[21] Naro A, Bramanti P, Leo A, Russo M and Calabrò R S 2016 Transcranial alternating current stimulation in patients with chronic disorder of consciousness: a possible way to cut the diagnostic gordian knot? *Brain Topogr.* **29** 623–44
[22] Xie Y, Zhang T and Chen A C N 2015 Repetitive transcranial magnetic stimulation for the recovery of stroke patients with disturbance of consciousness *Brain Stimul.* **8** 674–5
[23] Sanz Leon P, Knock S A, Woodman M M, Domide L, Mersmann J, McIntosh A R and Jirsa V 2013 The virtual brain: a simulator of primate brain network dynamics *Front. Neuroinform.* **7** 10
[24] Wang H E *et al* 2024 Virtual brain twins: from basic neuroscience to clinical use *Natl Sci. Rev.* **11** nwae079
[25] Li G *et al* 2021 Multiscale neural modeling of resting-state fMRI reveals executive-limbic malfunction as a core mechanism in major depressive disorder *NeuroImage: Clin.* **31** 102758
[26] Robinson P A, Rennie C J, Rowe D L, O'Connor S C and Gordon E 2005 Multiscale brain modelling *Phil. Trans. R. Soc. B* **360** 1043–50
[27] Breakspear M, Roberts J A, Terry J R, Rodrigues S, Mahant N and Robinson P A 2006 A unifying explanation of primary generalized seizures through nonlinear brain modeling and bifurcation analysis *Cereb. Cortex* **16** 1296–313
[28] Abeysuriya R G, Rennie C J and Robinson P A 2015 Physiologically based arousal state estimation and dynamics *J. Neurosci. Methods* **253** 55–69
[29] Assadzadeh S, Annen J, Sanz L, Barra A, Bonin E, Thibaut A, Boly M, Laureys S, Gosseries O and Robinson P A 2023 Method for quantifying arousal and consciousness in healthy states and severe brain injury via EEG-based measures of corticothalamic physiology *J. Neurosci. Methods* **398** 109958
[30] Polyakov D, Robinson P A, Makbili A, Gosseries O and Shriki O 2024 Neural field theory as a framework for modeling and understanding consciousness states in the brain *bioRxiv Preprint* https://doi.org/10.1101/2024.10.27.619702 (posted online 28 October 2024, accessed 10 March 2025)
[31] Sanz-Leon P, Robinson P A, Knock S A, Drysdale P M, Abeysuriya R G, Fung F K, Rennie C J and Zhao X 2018 NFTsim: theory and simulation of multiscale neural field dynamics *PLoS Comput. Biol.* **14** 1–37
[32] Wilson M T, Fung P K, Robinson P A, Shemmell J and Reynolds J N J 2016 Calcium dependent plasticity applied to repetitive transcranial magnetic stimulation with a neural field model *J. Comput. Neurosci.* **41** 107–25
[33] Wilson M T, Fulcher B D, Fung P K, Robinson P A, Fornito A and Rogasch N C 2018 Biophysical modeling of neural plasticity induced by transcranial magnetic stimulation *Clin. Neurophysiol.* **129** 1230–41
[34] Müller E J and Robinson P A 2018 Quantitative theory of deep brain stimulation of the subthalamic nucleus for the suppression of pathological rhythms in Parkinson's disease *PLoS Comput. Biol.* **14** 1–20
[35] Müller E J and Robinson P A 2018 Suppression of Parkinsonian beta oscillations by deep brain stimulation: determination of effective protocols *Front. Comput. Neurosci.* **12** 1–16
[36] Müller E J, Munn B R, Redinbaugh M J, Lizier J, Breakspear M, Saalmann Y B and Shine J M 2023 The non-specific matrix thalamus facilitates the cortical information processing modes relevant for conscious awareness *Cell Rep.* **42** 112844
[37] Xie Y and Zhang T 2012 Repetitive transcranial magnetic stimulation improves consciousness disturbance in stroke patients: a quantitative electroencephalography spectral power analysis *Neural Regen. Res.* **7** 2465–72
[38] Robinson P A, Rennie C J, Wright J J, Bahramali H, Gordon E and Rowe D L 2001 Prediction of electroencephalographic spectra from neurophysiology *Phys. Rev. E* **63** 0219031–02190318
[39] Robinson P A, Rennie C J, Rowe D L and O'Connor C 2004 Estimation of multiscale neurophysiologic parameters by electroencephalographic means *Hum. Brain Mapp.* **23** 53–72
[40] O'Connor S C and Robinson P A 2004 Spatially uniform and nonuniform analyses of electroencephalographic dynamics, with application to the topography of the alpha rhythm *Phys. Rev. E* **70** 19
[41] Rennie C J, Robinson P A and Wright J J 2002 Unified neurophysical model of EEG spectra and evoked potentials *Biol. Cybern.* **86** 457–71
[42] Rowe D L, Robinson P A and Rennie C J 2004 Estimation of neurophysiological parameters from the waking EEG using a biophysical model of brain dynamics *J. Theor. Biol.* **231** 413–33
[43] O'Connor S C and Robinson P A 2005 Analysis of the electroencephalographic activity associated with thalamic tumors *J. Theor. Biol.* **233** 271–86
[44] Fulcher B D, Phillips A J K and Robinson P A 2008 Modeling the impact of impulsive stimuli on sleep-wake dynamics *Phys. Rev. E* **78** 1–14
[45] Kerr C C, Rennie C J and Robinson P A 2008 Physiology-based modeling of cortical auditory evoked potentials *Biol. Cybern.* **98** 171–84
[46] Nevado-Holgado A J, Marten F, Richardson M P and Terry J R 2012 Characterising the dynamics of EEG waveforms as the path through parameter space of a neural mass model: application to epilepsy seizure evolution *NeuroImage* **59** 2374–92
[47] Robinson P A, Sarkar S, Pandejee G M and Henderson J A 2014 Determination of effective brain connectivity from functional connectivity with application to resting state connectivities *Phys. Rev. E* **90** 1–6
[48] Penfield W and Jasper H 1954 *Epilepsy and the Functional Anatomy of the Human Brain* (Brown)
[49] Nunez P L 1995 *Neocortical Dynamics and Human EEG Rhythms* (Oxford University Press)
[50] Braitenberg V and Schüz A 1998 *Cortex: Statistics and Geometry of Neuronal Connectivity* 2nd edn (Springer)
[51] Robinson P A, Rennie C J and Wright J J 1997 Propagation and stability of waves of electrical activity in the cerebral cortex *Phys. Rev. E* **56** 826–40
[52] Annen J *et al* 2023 Cerebral electrometabolic coupling in disordered and normal states of consciousness *Cell Rep.* **42** 112854

[53] Polyakov D 2024 Personalized stimulation therapies for disorders of consciousness - Code and Data (PLoS) *Zenodo* (https://doi.org/10.5281/zenodo.11212096)
[54] Pion-Tonachini L, Kreutz-Delgado K and Makeig S 2019 ICLabel: an automated electroencephalographic independent component classifier, dataset and website *Neuroimage* **198** 181–97
[55] Delorme A and Makeig S 2004 EEGLAB: an open source toolbox for analysis of single-trial EEG dynamics including independent component analysis *J. Neurosci. Methods* **134** 9–21
[56] Robinson P A, Rennie C J and Rowe D L 2002 Dynamics of large-scale brain activity in normal arousal states and epileptic seizures *Phys. Rev. E* **65** 9
[57] Abeysuriya R G, Rennie C J and Robinson P A 2014 Prediction and verification of nonlinear sleep spindle harmonic oscillations *J. Theor. Biol.* **344** 70–77
[58] Robinson P A, Phillips A J K, Fulcher B D, Puckeridge M and Roberts J A 2011 Quantitative modelling of sleep dynamics *Phil. Trans. R. Soc. A* **369** 3840–54
[59] Bhattacharya B S and Chowdhury F N 2015 *Validating Neuro- Computational Models of Neurological and Psychiatric Disorders* (Springer)
[60] Crick F and Koch C 1990 Towards a neurobiological theory of consciousness *Semin. Neurosci.* **2** 263–75 (available at: http://resource.nlm.nih.gov/101584582X469)
[61] Storm J F, Boly M, Casali A G, Massimini M, Olcese U, Pennartz C M A and Wilke M 2017 Consciousness regained: disentangling mechanisms, brain systems and behavioral responses *J. Neurosci.* **37** 10882–93
[62] Boly M, Massimini M, Tsuchiya N, Postle B R, Koch C and Tononi G 2017 Are the neural correlates of consciousness in the front or in the back of the cerebral cortex? Clinical and neuroimaging evidence *J. Neurosci.* **37** 9603–13
[63] Darracq M *et al* 2018 Evoked alpha power is reduced in disconnected consciousness during sleep and anesthesia *Sci. Rep.* **8** 1–10
[64] Stevner A B A *et al* 2019 Discovery of key whole-brain transitions and dynamics during human wakefulness and non-REM sleep *Nat. Commun.* **10** 1–14
[65] Goldfine A M, Victor J D, Conte M M, Bardin J C and Schiff N D 2011 Determination of awareness in patients with severe brain injury using EEG power spectral analysis *Clin. Neurophysiol.* **122** 2157–68
[66] Rosanova M *et al* 2012 Recovery of cortical effective connectivity and recovery of consciousness in vegetative patients *Brain* **135** 1308–20
[67] Schnakers C and Laureys S 2017 *Coma and Disorders of Consciousness* 2nd edn (Springer)
[68] Bai Y, Lin Y and Ziemann U 2021 Managing disorders of consciousness: the role of electroencephalography *J. Neurol.* **268** 4033–65
[69] Mediano P A M, Seth A K and Barrett A B 2019 Measuring integrated information: comparison of candidate measures in theory and simulation *Entropy* **21** 1–30
[70] Demertzi A, Schnakers C, Soddu A, Bruno M-A, Gosseries O, Vanhaudenhuyse A and Laureys S 2011 Neural plasticity lessons from disorders of consciousness *Front. Psychol.* **1** 1–7
[71] Bagnato S, Boccagni C, Sant'Angelo A, Fingelkurts A A, Fingelkurts A A and Galardi G 2013 Emerging from an unresponsive wakefulness syndrome: brain plasticity has to cross a threshold level *Neurosci. Biobehav. Rev.* **37** 2721–36
[72] Lynch M A 2004 Long-term potentiation and memory *Physiol. Rev.* **84** 87–136
[73] Abraham W C, Bliss T V P, Collingridge G L and Morris R G M 2024 Long-term potentiation: 50 years on: past, present and future *Phil. Trans. R. Soc. B* **379** 1–7
[74] Schmalz J and Kumar G 2019 Controlling synchronization of spiking neuronal networks by harnessing synaptic plasticity *Front. Comput. Neurosci.* **13** 1–17
[75] Turrigiano G 2012 Homeostatic synaptic plasticity: local and global mechanisms for stabilizing neuronal function *Cold Spring Harb. Perspect. Biol.* **4** 1–18
[76] Assadzadeh S and Robinson P A 2018 Necessity of the sleep-wake cycle for synaptic homeostasis: system-level analysis of plasticity in the corticothalamic system *R. Soc. Open Sci.* **5** 171952
[77] Shoob S *et al* 2023 Deep brain stimulation of thalamic nucleus reuniens promotes neuronal and cognitive resilience in an Alzheimer's disease mouse model *Nat. Commun.* **14** 7002 (accessed 10 March 2025)
[78] Tewarie P K B, Abeysuriya R, Laureys S, Deco G and Annen J 2024 Individual trajectories for recovery of neocortical activity in disorders of consciousness *bioRxiv Preprint* https://doi.org/10.1101/2024.03.11.584433 (posted online 13 March 2024)
[79] Fung P K and Robinson P A 2013 Neural field theory of calcium dependent plasticity with applications to transcranial magnetic stimulation *J. Theor. Biol.* **324** 72–83
[80] Gervais C, Boucher L-P, Villar G M, Lee U C and Duclos C 2023 A scoping review for building a criticality-based conceptual framework of altered states of consciousness *Front. Syst. Neurosci.* **17** 1085902
[81] Sanz-Leon P and Robinson P A 2017 Multistability in the corticothalamic system *J. Theor. Biol.* **432** 141–56
[82] Gosseries O *et al* 2015 On the cerebral origin of EEG responses to TMS: insights from severe cortical lesions *Brain Stimul.* **8** 142–9
[83] Nasr K, Haslacher D, Dayan E, Censor N, Cohen L G and Soekadar S R 2022 Breaking the boundaries of interacting with the human brain using adaptive closed-loop stimulation *Prog. Neurobiol.* **216** 102311
[84] Montgomery E B and Gale J T 2008 Mechanisms of action of deep brain stimulation (DBS) *Neurosci. Biobehav. Rev.* **32** 388–407
[85] Antal A and Paulus W 2013 Transcranial alternating current stimulation (tACS) *Front. Hum. Neurosci.* **7** 1–4
[86] Louise-Bender Pape T, Rosenow J, Lewis G, Ahmed G, Walker M, Guernon A, Roth H and Patil V 2009 Repetitive transcranial magnetic stimulation-associated neurobehavioral gains during coma recovery *Brain Stimul.* **2** 22–35
[87] Lemaire J J *et al* 2018 Deep brain stimulation in five patients with severe disorders of consciousness *Ann. Clin. Transl. Neurol.* **5** 1372–84
[88] Gogulski J *et al* 2023 Personalized repetitive transcranial magnetic stimulation for depression *Biol. Psychiatry: Cogn. Neurosci. Neuroimaging* **8** 351–60
[89] Thiele C, Zaehle T, Haghikia A and Ruhnau P 2021 Amplitude modulated transcranial alternating current stimulation (AM-TACS) efficacy evaluation via phosphene induction *Sci. Rep.* **11** 1–10
[90] Holt A B, Wilson D, Shinn M, Moehlis J and Netoff T I 2016 Phasic burst stimulation: a closed-loop approach to tuning deep brain stimulation parameters for Parkinson's disease *PLoS Comput. Biol.* **12** 1–14
[91] Guerrero Moreno J, Biazoli C E, Baptista A F and Trambaiolli L R 2021 Closed-loop neurostimulation for affective symptoms and disorders: an overview *Biol. Psychol.* **161** 108081
[92] Martens G *et al* 2021 A novel closed-loop EEG-tDCS approach to promote responsiveness of patients in minimally conscious state: a study protocol *Behav. Brain Res.* **409** 113311
[93] Cuschieri A, Borg N and Zammit C 2022 Closed loop deep brain stimulation: a systematic scoping review *Clin. Neurol. Neurosurg.* **223** 107516
[94] Pan J, Xiao J, Wang J, Wang F, Li J, Qiu L, Di H and Li Y 2022 Brain–computer interfaces for awareness detection, auxiliary diagnosis, prognosis and rehabilitation in patients with disorders of consciousness *Semin. Neurol.* **42** 363–74

[95] Spataro R, Xu Y, Xu R, Mandalà G, Allison B Z, Ortner R, Heilinger A, La Bella V and Guger C 2022 How brain-computer interface technology may improve the diagnosis of the disorders of consciousness: a comparative study *Front. Neurosci.* **16** 1–11
[96] Galiotta V *et al* 2022 EEG-based brain-computer interfaces for people with disorders of consciousness: features and applications. A systematic review *Front. Hum. Neurosci.* **16** 1–17
[97] Pan J *et al* 2020 Prognosis for patients with cognitive motor dissociation identified by brain-computer interface *Brain* **143** 1177–89
[98] Sebastián-Romagosa M, Cho W, Ortner R, Murovec N, Von Oertzen T, Kamada K, Allison B Z and Guger C 2020 Brain computer interface treatment for motor rehabilitation of upper extremity of stroke patients—a feasibility study *Front. Neurosci.* **14** 591435
[99] Polyakov D, Robinson P A, Müller E J and Shriki O 2024 Recruiting neural field theory for data augmentation in a motor imagery brain–computer interface *Front. Robot. AI* **11** 1–15
[100] Mayberg H S, Lozano A M, Voon V, McNeely H E, Seminowicz D, Hamani C, Schwalb J M and Kennedy S H 2005 Deep brain stimulation for treatment-resistant depression *Neuron* **45** 651–60
[101] Morishita T, Fayad S M, Higuchi M-A, Nestor K A and Foote K D 2014 Deep brain stimulation for treatment-resistant depression: systematic review of clinical outcomes *Neurotherapeutics* **11** 475–84